Microconnectomics of the Pretectum and Ventral Thalamus in the Chicken (*Gallus gallus*)

Tomas Vega-Zuniga,[1]* Gonzalo Marín,[2,3] Cristian González-Cabrera,[2] Eva Planitscher,[1] Anja Hartmann,[1] Vanessa Marks,[1] Jorge Mpodozis,[2] and Harald Luksch[1]

[1]Lehrstuhl für Zoologie, Technische Universität München, Freising-Weihenstephan, Germany
[2]Laboratorio de Neurobiología y Biología del Conocer, Departamento de Biología, Facultad de Ciencias, Universidad de Chile, Santiago, Chile
[3]Facultad de Medicina, Universidad Finis Terrae, Santiago, Chile

ABSTRACT

The avian pretectal and ventrothalamic nuclei, encompassing the griseum tectale (GT), n. lentiformis mesencephali (LM), and n. geniculatus lateralis pars ventralis (GLv), are prominent retinorecipient structures related to optic flow operations and visuomotor control. Hence, a close coordination of these neural circuits is to be expected. Yet the connectivity among these nuclei is poorly known. Here, using intracellular labeling and *in situ* hybridization, we investigated the detailed morphology, connectivity, and neurochemical identity of neurons in these nuclei. Two different cell types exist in the GT: one that generates an axonal projection to the optic tectum (TeO), LM, GLv, and n. intercalatus thalami (ICT), and a second population that only projects to the LM and GLv. *In situ* hybridization revealed that most neurons in the GT express the vesicular glutamate transporter (VGluT2) mRNA, indicating a glutamatergic identity. In the LM, three morphological cell types were defined, two of which project axons towards dorsal targets. The LM neurons showed strong VGluT2 expression. Finally, the cells located in the GLv project to the TeO, LM, GT, n. principalis precommisuralis (PPC), and ICT. All neurons in the GLv showed strong expression of the vesicular inhibitory amino acid transporter (VIAAT) mRNA, suggesting a GABAergic identity. Our results show that the pretectal and ventrothalamic nuclei are highly interconnected, especially by glutamatergic and GABAergic neurons from the GT and GLv, respectively. This complex morphology and connectivity might be required to organize orienting visuomotor behaviors and coordinate the specific optic flow patterns that they induce. J. Comp. Neurol. 524:2208–2229, 2016.

INDEXING TERMS: GLv; GT; LM; ICT; neurochemistry; slice; birds; biocytin; RRID:nlx_84100; RRID:nlx_84530; RRID:OMICS_02343

In vertebrates, retinal projections can be divided into six parallel central pathways: to the optic tectum (tectofugal), the dorsal thalamic complex (thalamofugal), the ventral thalamic complex, the suprachiasmatic nuclei, the accessory optic system, and the pretectal complex (Rodieck, 1979; Major et al., 2003; Butler and Hodos, 2005). In mammals and birds, research has been focused primarily on the thalamofugal (Reese and Cowey, 1983; Xu et al., 2001; Kaas and Lyon, 2007), tectofugal (Karten and Revzin, 1966; Luksch, 2003; Marín et al., 2003), suprachiasmatic nucleus (SCN) (Rusak and Zucker, 1979; Buijs and Kalsbeek, 2001; Cantwell and Cassone, 2006; Brandstätter and Abraham, 2003), and accessory optic system / pretectal pathways (Wylie et al., 1997; Wylie, 2001; Crowder et al., 2003). Functionally, the thalamo- and tectofugal pathways have been implicated in many different tasks such as color vision, stereopsis, spatial attention, and motion detection (Bishop and Pettigrew, 1986; Pettigrew, 1986; Frost et al., 1988; Marín et al., 2005; Wylie et al., 2009). The SCN is involved in circadian rhythms acting as a central clock (Stephan and Zucker, 1972;

Grant sponsor: Fondo Nacional de Desarrollo Cientifico y Technologico; Grant numbers: 1151432, 1120124.

*CORRESPONDENCE TO: Dr. Tomas Vega-Zuniga, Lehrstuhl für Zoologie, Technische Universität München, Liesel-Beckmann Str. 4, 85354 Freising, Germany. E-mail: tomas.vega-zuniga@tum.de

Received October 29, 2015; Revised November 23, 2015;
Accepted November 24, 2015.
DOI 10.1002/cne.23941
Published online December 23, 2015 in Wiley Online Library (wileyonlinelibrary.com)

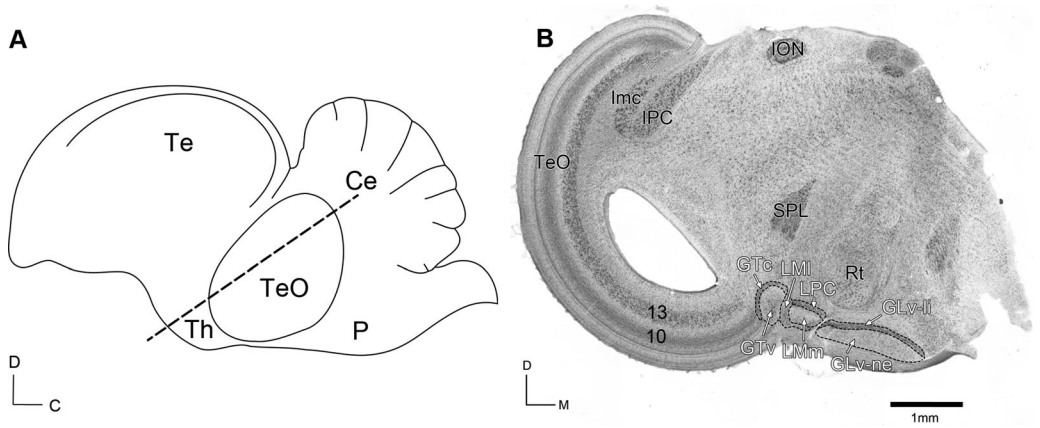

Figure 1. **A**: Schematic sagittal view of the chicken brain. Dashed line represents approximately the location of the section in B. D = dorsal; C = caudal. **B**: Giemsa staining of a 60-μm section showing the diencephalic structures griseum tectale (GTc, GTv), n. lentiformis mesencephali (LMl, LMm), and the n. geniculatus lateralis pars ventralis (GLv-li, GLv-ne) studied in the present work. D = dorsal; M = medial.

Bell-Pedersen et al., 2005). The accessory optic system (in birds referred to as nuclei of the basal optic root (nBOR)), on the other hand, has been implicated in optic flow and optokinetic responses that control eye stabilization (Simpson, 1984; McKenna and Wallman, 1985; Wylie and Frost, 1999). Conversely, the other retinal pathways, especially the ones that proceed to some pretectal nuclei (e.g., griseum tectale) and ventral thalamus, have been scarcely studied. This has led to a poor comprehension of the functionality of these nuclei, including their interaction with the main visual pathways. Therefore, to understand the role of these pretectal and ventrothalamic nuclei in vision, detailed morphological and microprojection pattern studies are needed.

In birds, the pretectum and ventral thalamus contains several retino-recipient structures. Some of these nuclei, the n. lentiformis mesencephali (LM), the n. geniculatus lateralis pars ventralis (GLv), and the griseum tectale (GT), share a prominent retinotopy (Crossland and Uchwat, 1979; Gamlin and Cohen, 1988a; Vega-Zuniga et al., 2014). Numerous evidence indicates that these nuclei are connected directly and/or indirectly to neural structures involved in visuomotor control (du Lac and Knudsen, 1990; Masino and Knudsen, 1993; Wylie, 2001) and corollary discharges which may flow through axonal branches connecting imminent motor responses with sensory pathways (Crapse and Sommer, 2008; Yang et al., 2008).

The LM is divided into a medial (LMm) and a lateral part (LMl) (Fig. 1) with separate retinotopic maps that are mirror images of each other (Gamlin and Cohen, 1988b; Wylie et al., 2014). Projections of the LM are directed to folia VI to IX of the cerebellum (Cb), inferior olive (OI), and the lateral and medial pontine nucleus (PL and PM) (Freedman et al., 1975; Clarke, 1977; Pakan et al., 2006; Iwaniuk et al., 2009; Wylie et al., 2009). Nonretinal afferents to the LM arises mainly from the nBOR, TeO, and GLv (Gamlin and Cohen, 1988b). Substantial evidence indicates that the LM along with the nucleus of the basal optic root (nBOR) are involved in optic flow and retinal image stabilization during self motion (Wylie and Frost, 1999; Wylie, 2000; Wylie and Crowder, 2000). Compared to other pretectal nuclei, the GT has attracted little attention over the years. Despite some reports (Gamlin and Cohen, 1988a,b), the functional role of this cell group remains obscure. The GT has a characteristic C-shaped form (in the anteroposterior axis) and is located medial to the optic tectum (TeO) and caudolateral to the LM. The GT is divided into three areas: griseum tectale pars compacta (GTc), griseum tectale pars ventralis (GTv) (Fig. 1), and griseum tectale pars dorsalis (GTd) (for details, see Gamlin and Cohen, 1988b). The major projections of the GT are to the n. intercalatus thalami (ICT), n. decussationis supraoptica ventrale (nDSV), and n. posteroventralis thalami (PV). The GT is also connected to the GLv and TeO. Nonretinal afferents to the GT arise mainly from the TeO (Gamlin and Cohen, 1988b). The GLv, on the other hand, is a conspicuous structure located dorsally to the optic tract and ventrally to the n. rotundus (Rt). It is composed of two main layers: a lamina interna (li) that contains tightly packed somata, and a neuropil (ne) (Fig. 1) with fewer cells that receives the retinal input (Crossland and Uchwat, 1979; Guiloff et al., 1987; Tömböl et al., 2004; Vega-Zuniga et al., 2014). Previous studies have shown that the GLv projects to the area pretectalis (AP), LM (Hu et al., 2004), and presumably to the n. pontis medialis (PM) (Marín et al., 2001). The PM in turn projects to

folia VIc–IXc in the cerebellum, which are related to visual and oculomotor responses (Freedman et al., 1975; Clarke, 1977). Nonretinal afferents to the GLv arise from the visual Wulst, TeO, GT, and VLT (Karten et al., 1973; Crossland and Uchwat, 1979; Vega-Zuniga et al., 2014). Although the role of the GLv is still unclear, it has been implicated in optokinetic reflex modulation and head and eye orienting movements (Pateromichelakis, 1979; Guiloff et al., 1987; Gioanni et al., 1991).

Apart from these general studies, detailed cellular morphology and connectivity of these nuclei both between them and with other visual structures remains unclear. This might be to some extent due to technical difficulties. As these nuclei are relatively small and rest deep in the avian brain, they are not easy targets for anatomical and physiological *in vivo* approaches. *In vitro* physiological experiments, on the other hand, have been focused on these nuclei separately, mainly because they are not easily included in the same slice (Guo et al., 2005, 2010). In this study, we used a slice preparation that preserves the tecto-pretecto-ventrothalamic connectivity, which allowed examination of these structures in great detail. We describe the morphology, projection pattern, and neurochemical identity of several main neuronal types that form these nuclei. We found that there is an intricate network of connections involving these structures, suggesting that these nuclei may form a functional unit implied in visuomotor tasks. Furthermore, the singular morphology and projection pattern of the neuronal types we have characterized may help to identify putative homologous neuronal populations in mammals and other vertebrate groups.

MATERIALS AND METHODS

Animals

One part of the experiment was conducted on 10 white leghorn chickens (*Gallus gallus*) of both sexes. Animals were obtained from a local dealer and maintained in an institutional facility. The ages of the animals ranged from P1 to P40. All surgical procedures used on these animals were approved by the University of Chile's Ethics Committee and conformed to National Institutes of Health guidelines on the ethical use of the animals. In addition, 35 white leghorn chick hatchlings (*Gallus gallus*; P1 until P3) were used for the *in vitro* experiments. Fertilized eggs were obtained from local breeders (Hatchery Hoelzl, Moosburg, Germany) and incubated at 37°C and 70% humidity. All *in vitro* procedures were approved by the Munich Veterinary Animal Care Committee and conformed to National Institutes of Health guidelines on the ethical use of the animals. All efforts were made to minimize both the suffering and number of animals used in these experiments.

Abbreviations

GLv	nucleus geniculatus lateralis pars ventralis
GLv-li	nucleus geniculatus lateralis pars ventralis – lamina interna
GLv-ne	nucleus geniculatus lateralis pars ventralis – neuropil
GT	griseum tectale
GTc	griseum tectale pars compacta
GTv	griseum tectale pars ventralis
ICT	nucleus intercalatus thalami
Imc	nucleus isthmi pars magno cellularis
ION	isthmo optic nucleus
Ipc	nucleus isthmi pars parvo cellularis
LM	nucleus lentiformis mesencephali
LMl	nucleus lentiformis mesencephali pars lateralis
LMm	nucleus lentiformis mesencephali pars medialis
LPC	nucleus laminaris precommissuralis
ot	optic tract
PPC	nucleus principalis precommissuralis
PT	nucleus pretectalis
Rt	nucleus rotundus
SO	stratum opticum
SPL	nucleus spiriformis lateralis
TeO	optic tectum

Slice preparations

Chick hatchlings were deeply anesthetized with a mixture (3:1) of ketamine (50 mg/ml; Inresa Arzneimittel, Germany) and Rompun (2%; Bayer, Germany), at 37.5 and 5 mg/kg, respectively, and subsequently decapitated. The skull was opened at the midsagittal line and the dorsal surface of the brain exposed. After removal, the brain was transferred into ice-cooled (4°C) sucrose-substituted Krebs solution (210 mM sucrose, 3 mM KCl (Sigma, St. Louis, MO), 3 mM $MgCl_2 \cdot 6H_2O$, 23 mM $NaHCO_3$, 1.2 mM $NaH_2PO_4 \cdot 6H_2O$ (Laborbedarf-Vertrieb, Germany), 11 mM D+-glucose). The forebrain and cerebellum were removed with cuts through the junction with the diencephalon and the cerebellar peduncles. The remaining parts of the brain were cut midsagittally into two hemispheres. The brain tissue was then embedded in low-melting agar at 48°C and rapidly cooled (1.5% Agar in HEPES solution: 290 mM sucrose, 3 mM KCl, 3 mM $MgCl_2$, and 5 mM HEPES; Sigma Chemical). The optic tectum of each hemisphere was aligned in an oblique transverse plane (for details see Vega-Zuniga et al., 2014). The hemispheres were cut into slices between 500–900 μm with a vibratome (VF 200 Compresstome, Precisionary Instruments, Greenville, NC). Slices were placed in standard artificial cerebrospinal fluid (ACSF) solution (120 mM NaCl, 3 mM KCl, 1 mM $MgCl_2 \cdot 6H_2O$, 23 mM $NaHCO_3$, 1.2 mM $NaH_2PO_4 \cdot 1H_2O$, 11 mM D+-glucose) and kept submerged in a chamber that was bubbled continuously with Carbogen (95% oxygen, 5% CO_2) at room temperature for at least 30 minutes.

In vitro extracellular injections

Pipettes were fabricated from borosilicate glass (GB100-8P, 0.58 × 1.00 × 80 mm; Science Products, Germany) with a one-stage microelectrode puller (P-97,

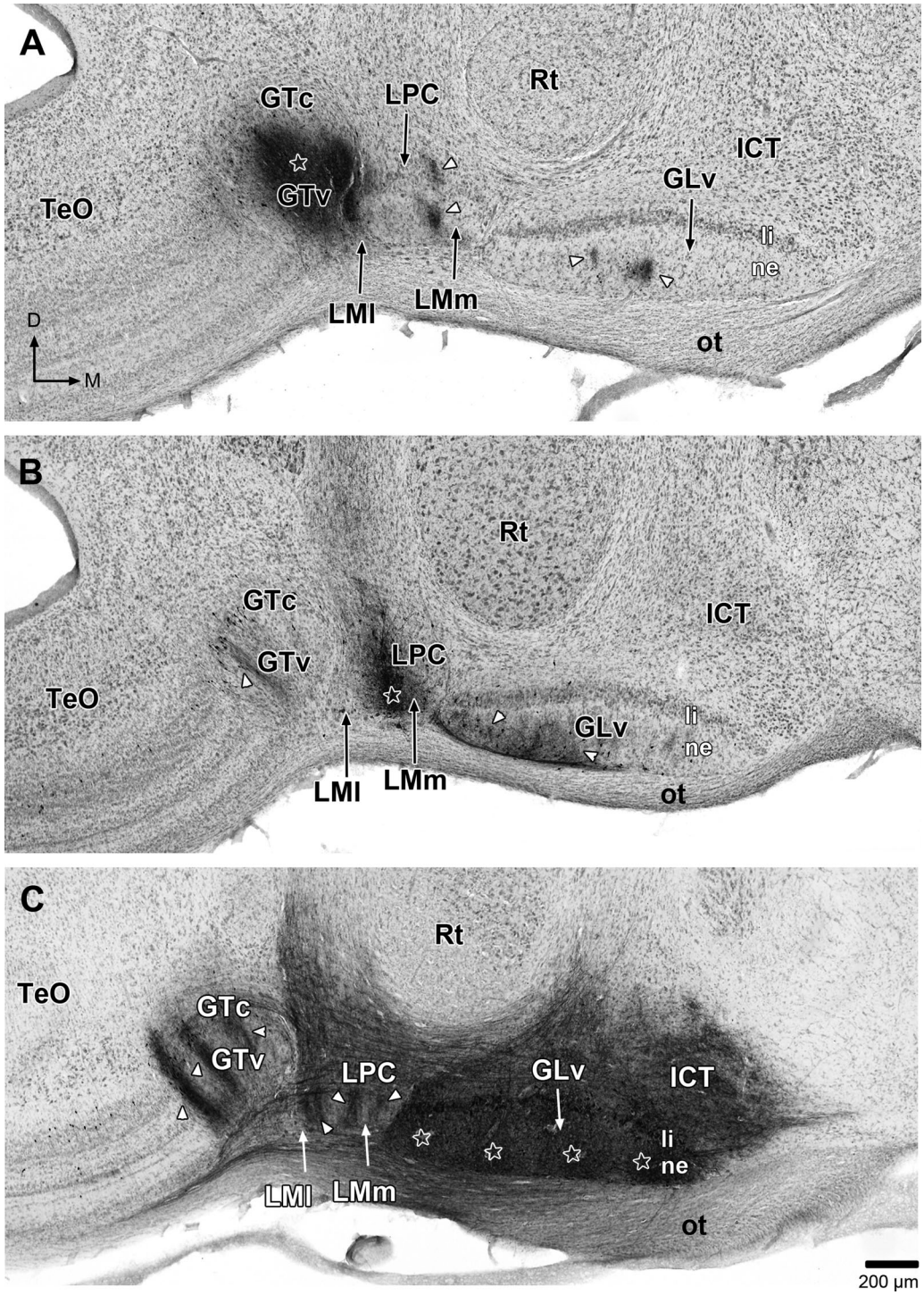

Figure 2. Giemsa staining of 60-µm sections showing anterograde and retrograde labeling of cells and processes (white arrowheads) in the pretectal and ventrothalamic region after *in vitro* biocytin injections into the GT **(A)**, LM **(B)**, and GLv **(C)**. Note the clear topographic labeling in the LM and GT after GLv injections (white arrowheads) (C). Asterisks indicate the injection(s) site. D = dorsal; M = medial. Scale bar in C applies to all.

Sutter Instrument, Novato, CA) to produce a tip opening around 30 µm. The electrodes were filled with mineral oil and attached to a Nanoliter 2000 injector (World Precision Instruments, New Haven, CT). Electrodes were filled with Biocytin 10% (hydrochloride, Sigma-Aldrich, Germany) dissolved in Tris-buffer 0.05 M (pH 10). Single slices were submerged in a chamber with carbogenated ACSF solution. Under microscopic

TABLE 1.
Sequences of PCR Primers Used to Amplify Specific cDNA Sequences of Each Marker

	Primer forward	Primer reverse	Annealing (°C)	Fragment (bp)
VGluT2	5′-GGCTCTGCACGCCGTCTCTC-3′	5′-TCGATGGTGTCCCCGGGCTT-3′	61.5	317
GLYT2	5′-TGCTGGCATCATCAGTGTACGGC-3′	5′-ACTGTACCTCGCAACCACAGCA-3′	61	384
VIAAT	5′-GGCTCTGCACGCCGTCTCTC-3′	5′-TCGATGGTGTCCCCGGGCTT-3′	61	425

control and using a microdrive (MaerzHaeuser, Germany), injections of 13.8 nL tracer solution in different positions along the GT, LM, and GLv were performed (Fig. 2). After injecting, slices were incubated 4 hours in carbogenated ACSF solution to allow transport of the tracer. Slices containing biocytin backfills were fixed overnight in 4% paraformaldehyde in 0.1M phosphate buffer (PFA/PB), transferred to 30% sucrose solution (in PB) for 2 hours, and sectioned to 60 μm on a cryotome (Kryostat 1720, Leitz, Germany). To visualize the staining, a heavy-metal-intensified DAB protocol was applied. Sections were first incubated in H_2O_2 solution (3% (wt/vol) H_2O_2) for 30 minutes to block endogenous peroxidase. After washing eight times (8 × 10 minutes) in PB 0.1M until oxygen bubbles disappeared, sections were incubated in 0.1% (vol/vol) avidin-biotinylated horseradish peroxidase (HRP) complex (ABC) solution containing 0.5% (vol/vol) Triton X-100 for 2 hours. Afterwards, samples were incubated in 0.026% diaminobenzidine / Ni-Co with 0.03% H_2O_2 for 6 minutes. Sections were mounted onto gelatin-subbed slides, counterstained with Giemsa (Sigma-Aldrich, Germany), dehydrated in an ethanol series ending in xylol, and coverslipped with DPX (Sigma-Aldrich, Germany).

In vitro intracellular filling

Electrodes were fabricated from borosilicate glass (GB150 F-8P, 0.86 × 1.50 × 80 mm, filament; Science Products, Germany) with a two-stage microelectrode puller (DMZ Universal) to produce electrodes with a resistance of 40–60 MΩ. The electrodes were filled with a mixture of 5% biocytin (hydrochloride, Sigma-Aldrich, Germany) and 0.5% sulforhodamine 101 (Sigma-Aldrich, Germany) dissolved in 0.05M Tris-buffer (pH 7.4) with 0.5M KCl. After incubation in acridin orange (10 mM, Sigma-Aldrich, Germany) for at least 20 minutes, single slices were transferred into a custom-built submerged slice chamber on a microscope stage that was continuously perfused with ACSF solution (RT 21/22°C); slices were stabilized with a U-shaped platinum wire. Sharp electrodes were moved through the tissue using a micromanipulator (MWS-1A Narishige, Japan) under an epifluorescent microscope (NikonY-FL, Eclipse E600FN, Japan). Once a cell was impaled, biocytin/rhodamine was injected into the cell with a positive current of 0.8 nA for 5 minutes. After a successful filling corroborated with rhodamine fluorescence, slices were incubated for 3 hours in carbogenated ACSF solution; then fixed overnight in 4% paraformaldehyde in 0.1M phosphate buffer (PFA/PB), transferred to 30% sucrose solution (in PB) and cut into 75-μm sections with a cryotome (Kryostat 1720, Leitz, Germany). To visualize the neurons filled with biocytin, a slightly adapted heavy-metal-intensified DAB protocol was applied. Sections were first incubated in H_2O_2 solution (3% (wt/vol) H_2O_2) for 30 minutes to block endogenous peroxidase. After washing eight times (8 × 10 minutes) in PB 0.1M until oxygen bubbles disappeared, slices were incubated in 0.5% (vol/vol) avidin-biotinylated HRP complex (ABC) solution containing 0.5% (vol/vol) Triton X-100 overnight. Afterwards, samples were incubated in 0.026% diaminobenzidine Ni-Co for 10 minutes. The chromogenic reaction was achieved by adding H_2O_2 (final concentration 0.01%) for 60 seconds. Finally, sections were mounted onto gelatin-subbed slides, counterstained with Giemsa (Sigma-Aldrich, Germany) dehydrated, and coverslipped in DPX as mentioned above.

RNA probes and primers design

RNA probes were designed using the chicken (*Gallus gallus*) nucleotide databases (NCBI Nucleotide, RRID:nlx_84100) and the alignment tools of the NCBI website (NCBI BLAST, RRID:nlx_84530; Primer-BLAST, RRID:OMICS_02343; http://www.ncbi.nlm.nih.gov). To amplify the cDNA corresponding to each probe, specific pairs of primers (Table 1) were designed and commercially synthesized (IDT DNA, Skokie, IL). The selected transcript regions for each probe were the following: vesicular amino acid transporter (VIAAT): XM_417347, 425bp from nucleotide 515 to 939; glycine transporter (GLYT2): XM_420906.3, 384bp from nucleotide 117 to 500; vesicular glutamate transporter (VGluT2): NM_001168383, 317bp from nucleotide 14 to 330. Each chosen region was located in the coding region of its correspondent mRNA.

RNA extraction

Total RNA was isolated from the mesencephalon of chicken ranging from P5 until P15. Brain tissue was homogenized in 1 ml of RNAsolv Reagent (Omega

Biotek, Norcross, GA) using a dounce homogenizer, mixed with 0.2 ml of chloroform, and vortexed for 15 seconds. The mixture was then incubated for 10 minutes on ice and centrifuged at 10,000 RPM for 10 minutes at room temperature (Eppendorf, Germany, 5424 tabletop centrifuge). The aqueous phase was recovered, mixed with 0.5 ml of isopropyl alcohol, and incubated for 10 minutes prior to centrifugation at 10,000 RPM for 10 minutes at room temperature. The precipitated RNA pellet was washed with 1 ml of 80% ethanol, centrifuged at 8,500 RPM for 5 minutes at room temperature, air dried, and reconstituted with 70 μl of Nuclease free water.

Reverse-transcription polymerase chain reaction (RT-PCR)

Single strand cDNA was synthesized using Improm-II reverse transcriptase (Improm-IITM Reverse transcriptase, Promega, Madison, WI) according to the manufacturer's instructions. Briefly, 1 μg of total RNA and 1 μl of oligo(dT) primer were incubated for 5 minutes at 70°C with a reverse-transcription cocktail (1 μl reverse transcriptase; 2.5 μl 25 mM $MgCl_2$; 1 μl RNAse inhibitor RNAsin, Promega; 1 μl 10 mM mixed DNTPs; 4 μl of 5× reaction buffer), and then incubated at 42°C for 60 minutes. The obtained cDNA served as template in PCR reactions using Taq polymerase (Go-Taq, Promega). PCR protocols comprised 35 amplification cycles (denaturation 30 seconds at 94°C; annealing 60 seconds at temperature; extension 50 seconds at 72°C; and finalized by a single 10 minutes extension at 72°C). PCR products were analyzed in 1.5% agarose gels. Expected DNA fragments were excised from the gel and purified using a commercial kit (Wizard SV Gel and PCR clean-up system, Promega) according to the manufacturer's instructions.

Cloning

The four specific double-strand DNA sequences obtained were cloned into amplification vectors (p-GEMT easy vector, Promega) according to manufacturer's protocol. Heat competent DH5α bacteria were transformed by thermal shock (42°C for 90 seconds) and seeded onto Petri dishes with LB-Agar-XGal media (2.5% LB Broth, MO BIO, Carlsbad, CA; 2% agar, Bacto Agar, Sparks, MD; 40 μg/mL XGAL, US Biological, Swampscott, MA). Positive clones (selected by blue/white screening) were amplified in liquid LB-Ampicillin media (Ampicillin, US Biological) at 37°C for 16 hours. Cells were pelleted by centrifugation (13,000 RPM) and plasmidial DNA was purified using a commercial miniprep kit (QIAprep spin miniprep kit, Qiagen, Valencia, CA). Purified DNA was commercially sequenced (Sequencing Service, P. Universidad Católica de Chile) and compared to published sequences.

RNA probes synthesis

To obtain template DNA for RNA probes synthesis, purified plasmidial DNA was linearized by HincII or ZraI (Fermentas, Vilnius, Lithuania) restriction enzymes generating a sense or antisense template according to the orientation of the inserted fragment in the plasmid. For each probe, 5 μg of DNA was digested with 20 units of enzyme at 37°C for 16–20 hours in a final reaction volume of 100 μl. Linearized DNA was purified with a commercial kit (Wizard SV Gel and PCR clean-up system, Promega) and used as template for RNA probes synthesis. All probes used are full length.

Digoxigenin labeled RNA probes were synthesized *in vitro* using SP6 and T7 RNA polymerases (Riboprobe *in vitro* transcription systems, Promega) and digoxigenin labeled ribo-nucleotides (Dig RNA labeling mix 10×, Roche, Mannheim, Germany). Transcription mix (1 μg linearized DNA; 1 μl 100 mM DTT; 1 μl RNasin; 1 μl 10 mM (each) ribo-nucleotides mix; 4 μl 5× transcription buffer; 1 μl SP6 or T7 enzyme) was incubated for 2 hours at 37°C. Finally, RNA digoxigenin probes were purified with a commercial kit (E.Z.N.A. RNA Probe purification kit, Omega Biotek) and stored at −80°C.

In situ hybridization

Six chickens age 2–4 weeks old were perfused transcardially under deep anesthesia (ketamine 75 mg/kg, xylazine 5 mg/kg) using 300 ml of saline solution (NaCl 0.75%) followed by 250 ml of fixative (0.01 M phosphate buffer pH 7.4; 0.75% NaCl; 4% paraformaldehyde). Brains were removed and incubated in cryoprotective/postfixative solution (30% sucrose; 4% paraformaldehyde in DEPC-treated water) for 24–48 hours at 4°C. Once the brains had sunk they were mounted on a freezing sliding microtome (Leitz 1400) and cut in coronal sections of 80–100 μm. Free-floating sections were washed three times in phosphate-buffered saline (PBS; 0.01M phosphate buffer pH 7.4; 0.02% NaCl in DEPC-treated water) and treated with peroxide-PBS-T solution for 30 minutes (6% hydrogen peroxide; 0.1% Tween-20; Promega). The sections were then incubated in proteinase k-PBST solution (Proteinase K 10 μg/ml, Promega) for 10 minutes at room temperature (after testing different incubation times for optimal permeabilization), washed once in PBST, fixed in 4% PFA-PBST for 20 minutes, washed three times in PBST, and prehybridized at 65°C in hybridization buffer for 3 hours (50% formamide, Merck, Darmstadt, Germany; 1.3× SSC pH 5.3, Winkler, Santiago, Chile; 5 mM EDTA, Winkler; 200 μg/

ml tRNA from salmon sperm; 0.002% Tween-20; 0.005% CHAPS, Calbiochem, La Jolla, CA; 100 μg/ml heparin, Calbiochem). After adding the specific RNA probes and incubating for 16–18 hours at 65–70°C, the sections were washed twice in solution A (5× SSC pH 5.3; 50% formamide; 1% SDS) at 65°C for 30 minutes and three times in solution B (2.5× SSC pH 5.3; 50% formamide; 1% Tween-20) at 65°C for 30 minutes. After two washes in maleic acid buffer solution (MABT; 100 mM maleic acid, Sigma; 150 mM NaCl; 0.1% Tween-20) the sections were incubated in blocking solution (2% Blocking Reagent, Roche, Indianapolis, IN; 2% heat inactivated normal goat serum, in MABT) for 4 hours at room temperature and then incubated for 16–20 hours at 4°C with anti-digoxigenin-AP Fab fragments (1/1,000 dilution in MABT; Roche Diagnostics; RRID:AB_514497). Finally, the sections were washed six times in MABT, incubated in alkaline reaction buffer (100 mM Tris pH 9.5; 50 mM $MgCl_2$; 100 mM NaCl; 1% Tween-20), and developed at room temperature by adding NBT/BCIP reagent (NBT 375 μg/ml; BCIP 188 μg/ml; Stock Solution, Roche, Mannheim, Germany).

RESULTS

Extracellular injections in the pretectum and ventral thalamus

To investigate in detail the pretecto-ventrothalamic connectivity, oblique transverse slices that contained tectum, pretectum, and thalamus were prepared. For the pretectal structures we followed the Gamlin and Cohen nomenclature (1988a), namely, the griseum tectale – pars ventralis and compacta (GTv, GTc)-, the n. lentiformis mesencephali pars lateralis (LMl) and pars medialis (LMm), and the nucleus laminaris precommissuralis (LPC). This latter structure is located above the LMm and appears to be contiguous with the GLv-li (Fig. 1). The dorsal aspect of the GT and LM is not present in this slice preparation. It is important to mention that only the GTv, LMl, LMm, and GLv-ne are in receipt of retinal terminals (Crossland and Uchwat, 1979; Gamlin and Cohen, 1988a).

To ensure that the microcircuitry connecting the main nuclei was included in the slices, small extracellular biocytin injections were made in the GT, LM, and GLv (Fig. 2). After injections in the GT (Fig. 2A), retrogradely labeled cells were only observed in the GLv-ne. These cells were distributed in a small and limited area. Restricted GT terminal fields were observed in the LM and GLv-ne. In the TeO, GT terminals extended through layer 13 running perpendicular to the radial organization of the TeO without a clear topographic organization.

Injections in the LM (Fig. 2B) showed labeled neurons in the adjacent LPC. Retrogradely labeled cells were observed mainly in the GTc and almost half of the GLv- (ne, li). Some dispersed neurons were observed in the TeO. Also, neural processes were observed in the GLv, GT, and PPC.

After performing a series of contiguous small injections into the GLv (Fig. 2C), a widespread labeling pattern was observed throughout the ventral thalamus, pretectum, and tectum. These injections showed regularly spaced terminal zones in the LM, revealing a clear topographic arrangement of neural processes. In addition, retrogradely labeled cells in the GTc were grouped and regularly spaced with a clear topographic pattern. The TeO also showed labeled somata mainly in layer 10. Furthermore, labeled fibers were massively observed throughout the ICT and the surrounding ventrothalamic area that included the pretectal PPC and deep layers of the TeO. However, in these latter structures no clear topographic organization was observed (Fig. 2C).

Intracellular filling of the pretectum and ventral thalamus

To clarify the morphology and microcircuitry between these structures, intracellular cell fillings in the respective nuclei were made *in vitro*. Intracellular experiments in the GT lead to the identification of two different cell populations: GT-Type I cells (five cases; Fig. 3) located in the GTc and GTv had small somata with ventral dendritic processes that extended into the GTv, and dorsal t-shaped axons located above the GTc (Fig. 3A,B) that ran in the mediolateral direction from the TeO until the ICT. The lateral branch projected through the deep tectal layer 13 and generated two different terminal endings (along the mediolateral axis): the first one extended between layers 10–13 (Fig. 3C,D) and the second ended further lateral in layer 13 (Fig. 3E). The medial branch ran near the tectothalamic tract where it split into additional branches (Fig. 3F) that generated conspicuous terminal zones in the LMm (Fig. 3G) and ICT (Fig. 3H). GT-Type II cells (three cases; Fig. 4) located in the GTc had small somata with two main dendritic processes that extended dorsoventrally above the GTc and into the GTv. The axon arose from the ventral dendritic process (Fig. 4A) and ran through the mid LMm, where it formed a collateral terminal in the dorsal part of the LMm (Fig. 4C,D). The axon continued to the GLv through the optic tract, where it showed two separated and restricted neuropil terminal zones in the GLv: one lateral (Fig. 4E,F) and the other medial (Figs. 4G,H, 5C).

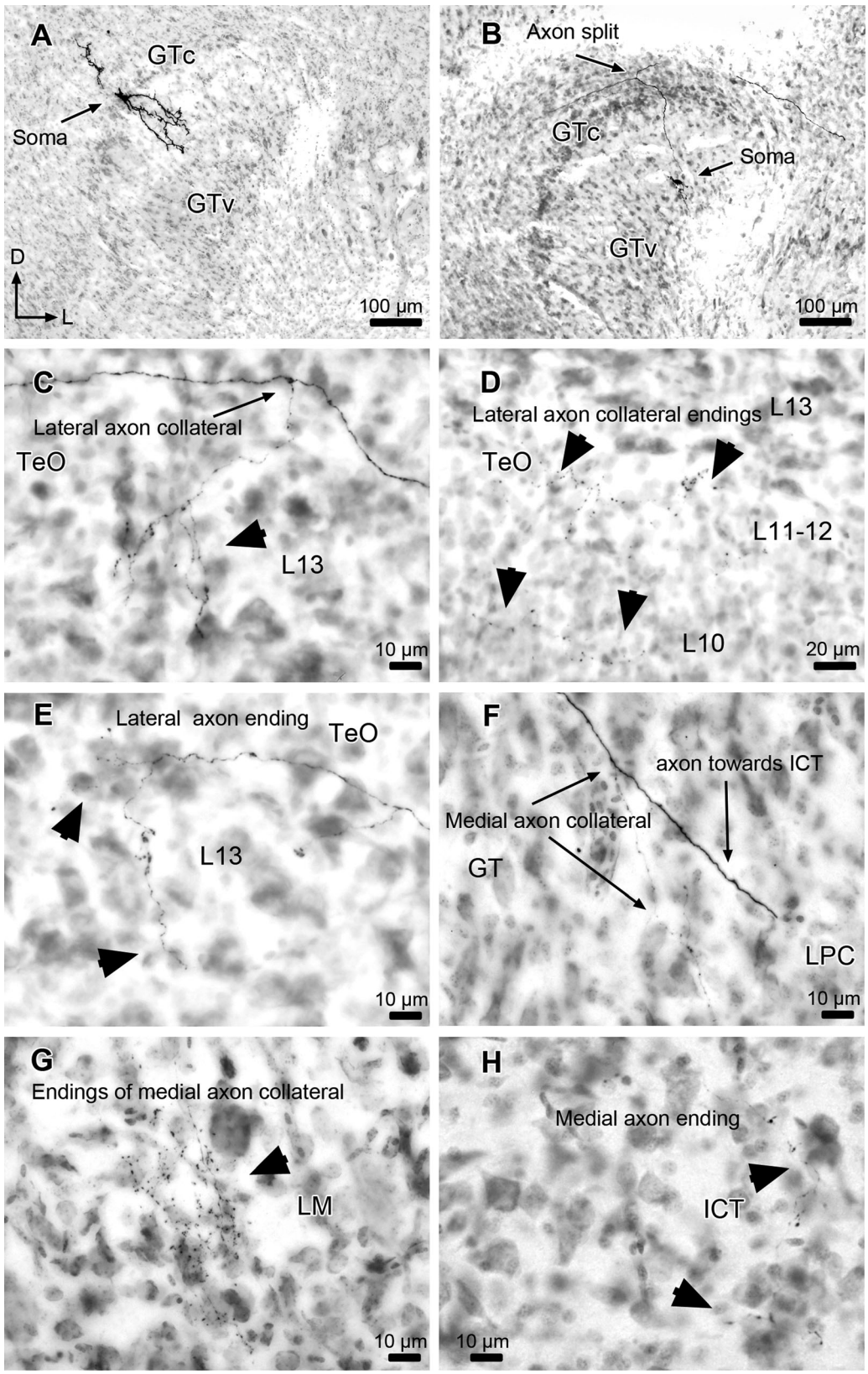

Figure 3. **A,B**: Intracellular filling of two representative GT type I cells located in the GTc and GTv. **C–H**: The axon and terminals in the different mesodiencephalic targets of the GT type I cells. Arrowheads show terminals in the respective nuclei. Note that the tectal axon collateral ends between layers 10–13 (C–E).

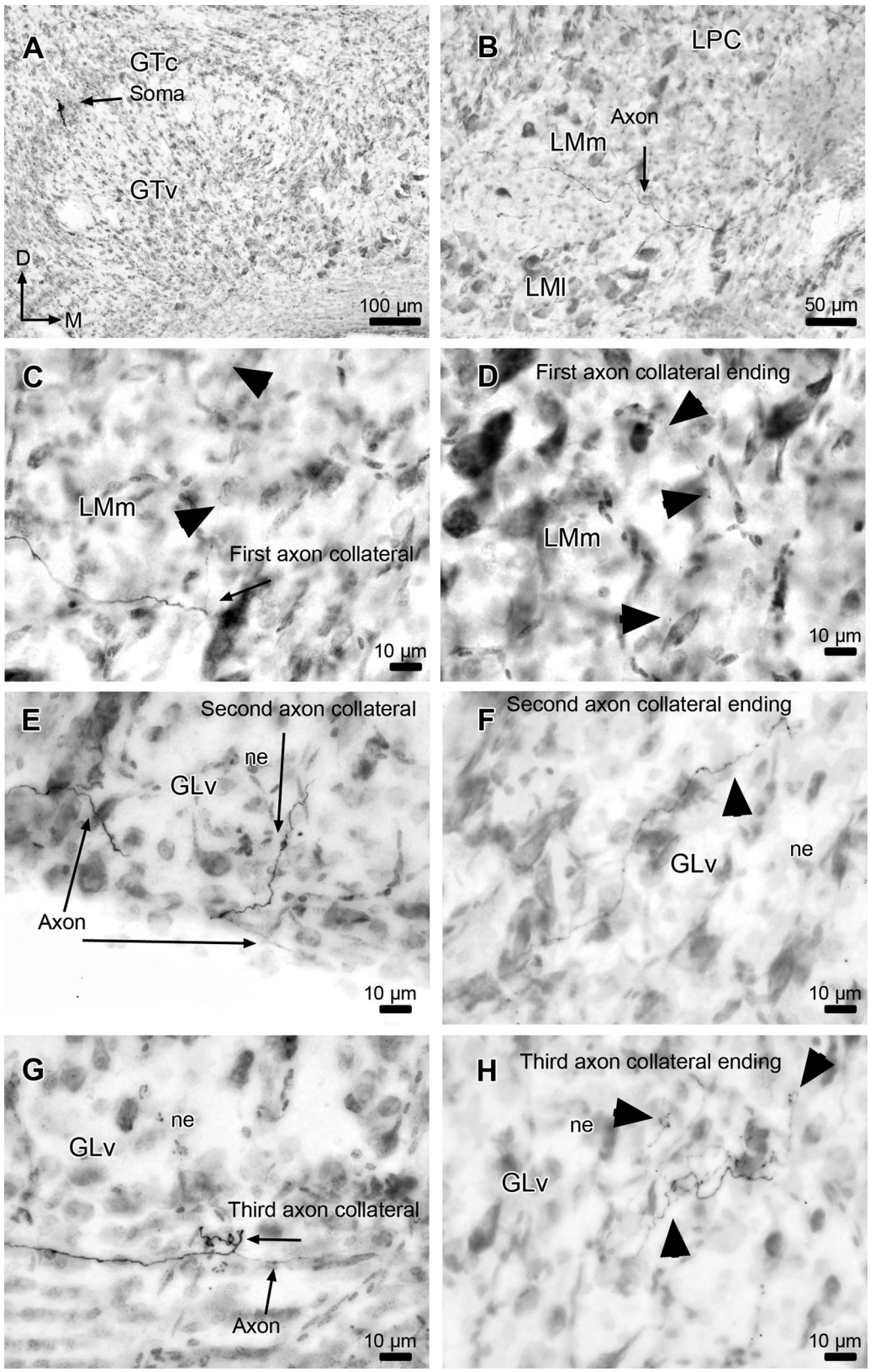

Figure 4. Intracellular filling of a representative GT type II cell located in the GTc **(A). B–H**: The axon and terminals in the different mesodiencephalic targets of the GT type II cell. Arrowheads show terminals in the respective nuclei. Note that the axon runs ventrally and that there is no tectal projection.

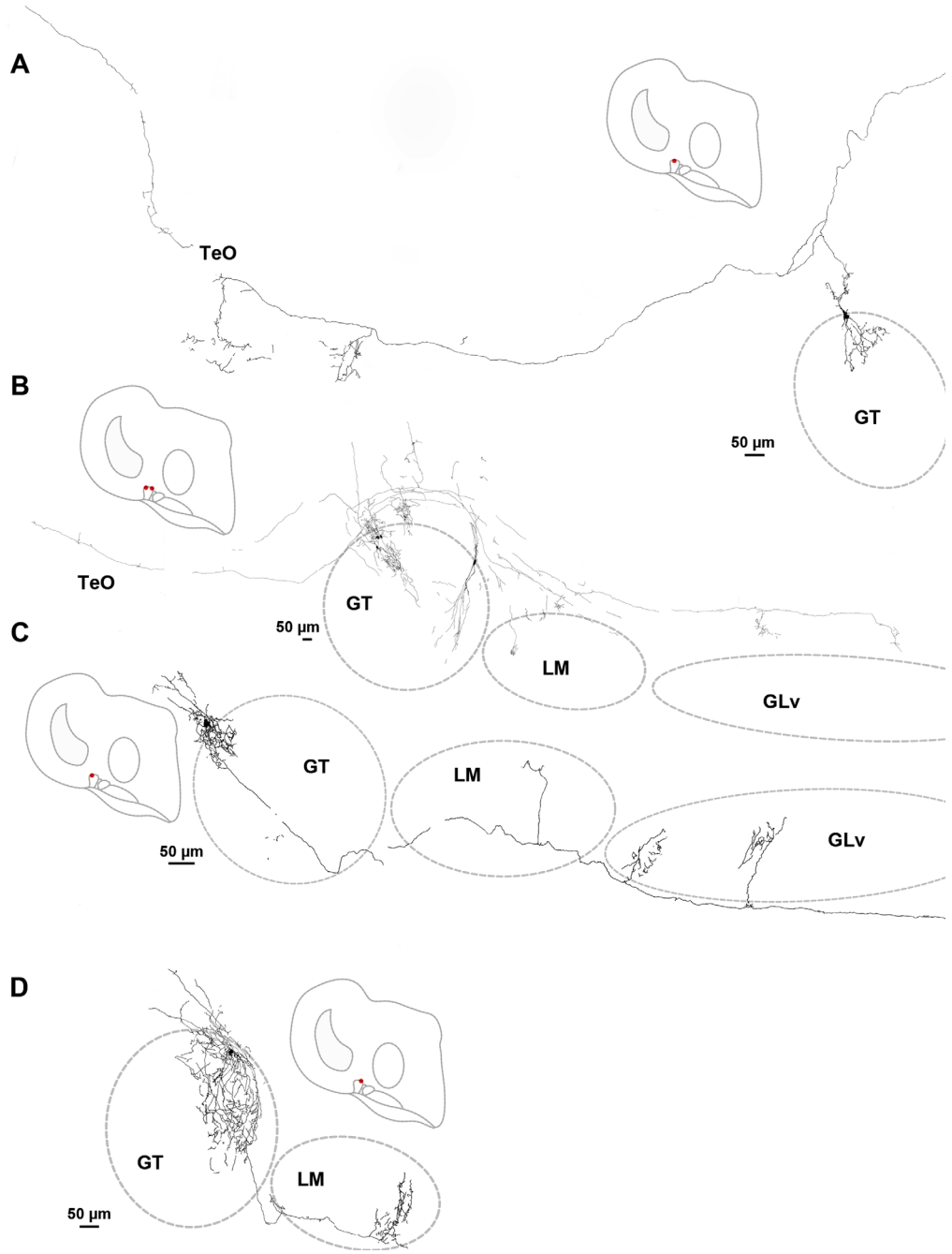

Figure 5. Reconstruction of biocytin-filled neurons in the GT. **A,B**: Type I neurons showing a characteristic dorsal axon that extends laterally into layers 10–13 of the TeO and medially to the LM and above the GLv. **C,D**: Type II neurons showing a ventral axon that runs through the optic tract ending in the LM and GLv. Insets with the dots indicate the location of each cell in the slice. [Color figure can be viewed in the online issue, which is available at wileyonlinelibrary.com.]

Intracellular fillings in the LM region (three cases; Fig. 6) revealed the identification of three different cell types. LM-Type I cells (three cases; Figs. 6C, 7A) were located in the LMm and had small somata with ventral dendritic fields. The axon emerged from one of the principal dorsal neurites and extended dorsally beyond the slice limits. LM-Type II cells (two cases; Figs. 6D, 7B) were located in the LMl between the GT and LMm. These neurons had big round somata with three main dendritic branches that extended dorsally, laterally, and ventrally, respectively. The dorsal and lateral dendritic arborization fields extended through the LMl. The medial dendritic arborization field extended to the LMm. The axon emerged from the dorsal dendrite

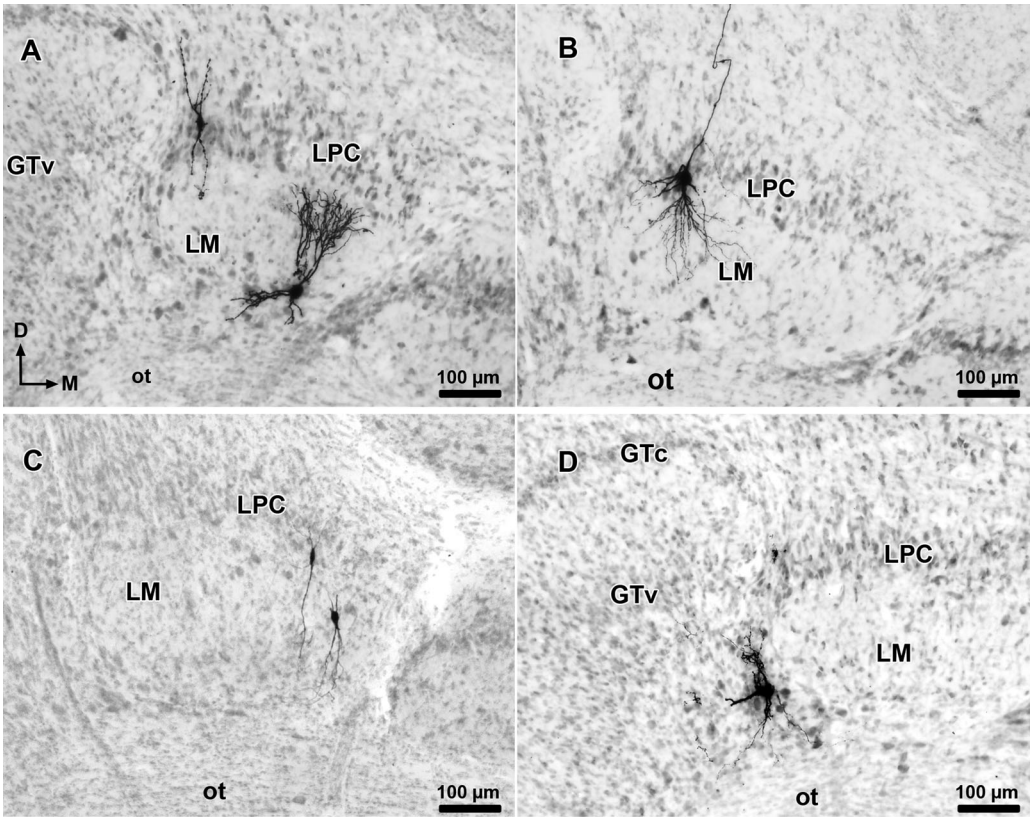

Figure 6. Intracellular filling of different cell types in the LM and LPC. **A**: LPC-Type I bipolar cell and a LM-type III cell located in the LMl with marked bipolar dendritic branches into the LMm. **B**: LPC-Type II cell showing a wide apical dendritic branch. **C**: LM-Type I cell located in the LMm. **D**: LM-Type II cell located in the LMl.

towards more distant regions beyond the slice limits. LM-Type III cells (three cases; Figs. 6A, 7C) were located in the ventral LMl, which at this level is placed below the LMm (Fig. 1). These neurons had big round somata with two prominent and dense bipolar dendritic fields. The dorsal arborization extended into the LMm and the ventral part covered the ventral LMl. There was no clear axon emerging from any of the neurites.

Additionally, we report two cell types in the dorsally adjacent structure to the LMm, the LPC (Fig. 1). We included these cells because we found an intrinsic morphological relationship between the LPC and LMm. LPC-Type I cells (two cases; Figs. 6A, 7D) had small somata with narrow bipolar dendritic arborization fields that had two branches each. The axon emerged from one of the dorsal dendrites and extended dorsally towards more distant regions beyond the slice limits. LPC-Type II cells (two cases; Figs. 6B, 7E) had round somata with wide and dense ventral dendritic fields that extended across more than half of the LMm. The axon emerged dorsally from one of the principal neurites and extended dorsally beyond the slice limits. In both cell types the ventral dendrites reached the retinorecipient LMm.

Regarding the GLv, we focused the intracellular filling experiments in the GLv-li (10 cases; Fig. 8) where projection neurons have been described. We were able to identify one characteristic cell type with a complex morphology and an axonal projection pattern that extended throughout several nuclei. These neurons (Fig. 8A) possessed small somata with two highly ramified dendritic fields: one extended ventrally into the GLv-ne where retinal projections terminate, and a second dendritic field reached dorsally, in and above the GLv-li, giving rise to an axon that split into two main branches in the region below Rt (Fig. 8B). The first branch projected medially and divided above the medial GLv, generating a collateral with a conspicuous terminal field into ICT (Fig. 8C); the other axon collateral ran mediodorsally, between Rt and ansa lenticularis (AL) towards more distant regions (Fig. 9A,C). The second axonal branch coming from the main dendrite proceeded laterally and generated several collaterals with terminal fields into the LMm/LMl (Fig. 8E), PPC (Fig. 8G), and layer 13 of the TeO (Figs. 8H, 9A–C).

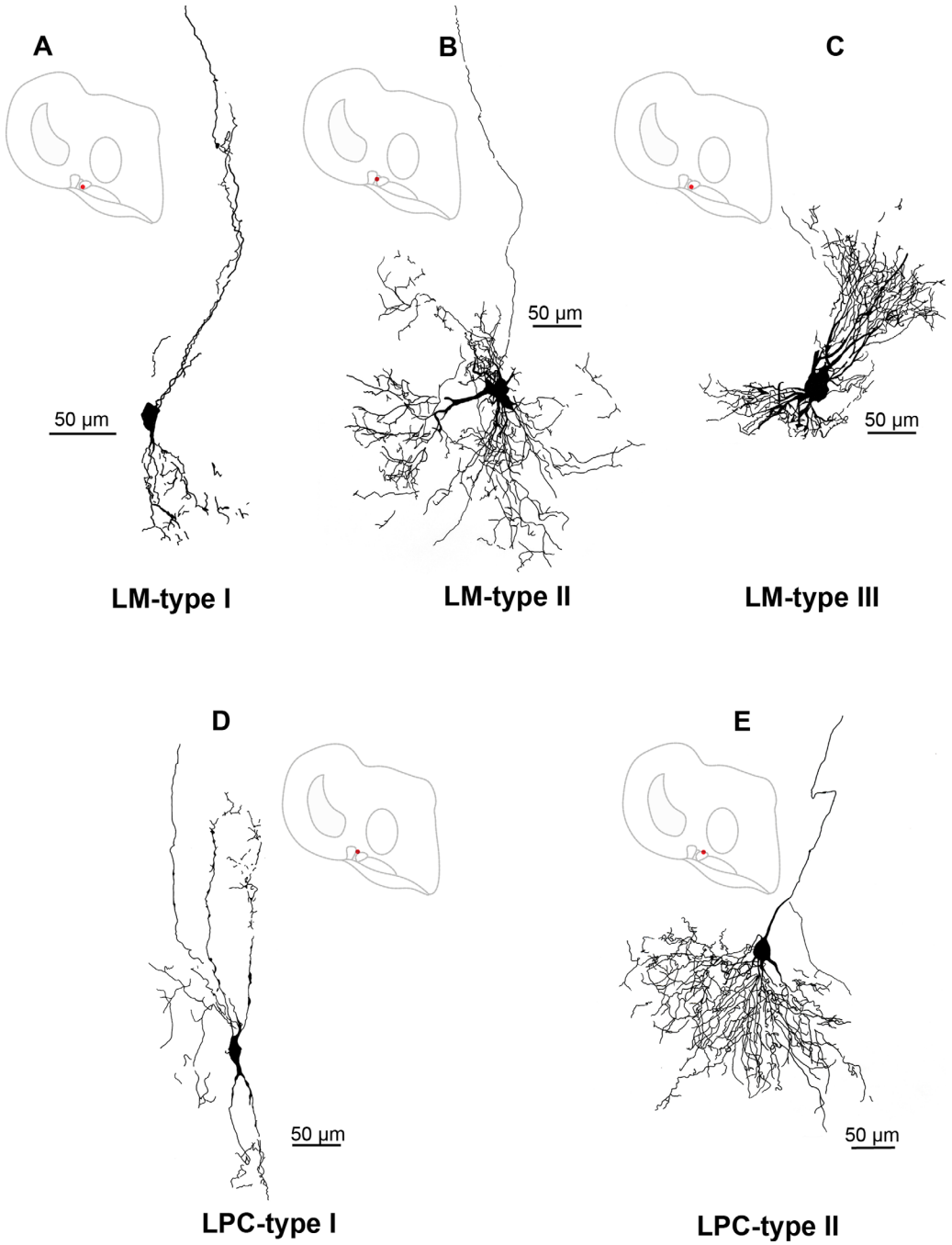

Figure 7. Reconstruction of biocytin-filled neurons in the LMm, LMl, and LPC. **A**: LM-Type I cell located in the medial LM with an axon extending dorsally. **B**: LM-Type II cell located in the LMl with three marked dendritic branches and an axon extending dorsally. **C**: LM-Type III cell located in the LMl with a marked and ramified bipolar dendritic arbor. **D**: LPC-Type I cell with a bipolar dendritic arbor and an axon extending dorsally. **E**: LPC-Type II cell with a wide dendritic arbor into the LMm and an axon extending dorsally. Insets with the dots indicate the location of each cell in a schematic slice. [Color figure can be viewed in the online issue, which is available at wileyonlinelibrary.com.]

Remarkably, in five cases we found an axon collateral of the lateral branch that formed a fine auto-terminal feeding back into the GLv-ne with conspicuous varicosities, adjacent to the main ventral dendritic branch (Fig. 8B,D).

In situ hybridization

In situ hybridization assays for VGluT2 ($n = 3$) and VIAAT ($n = 3$) were performed in transverse brain sections of chickens. As no differences were observed across the age range (P1–P40), the data are presented as a single group.

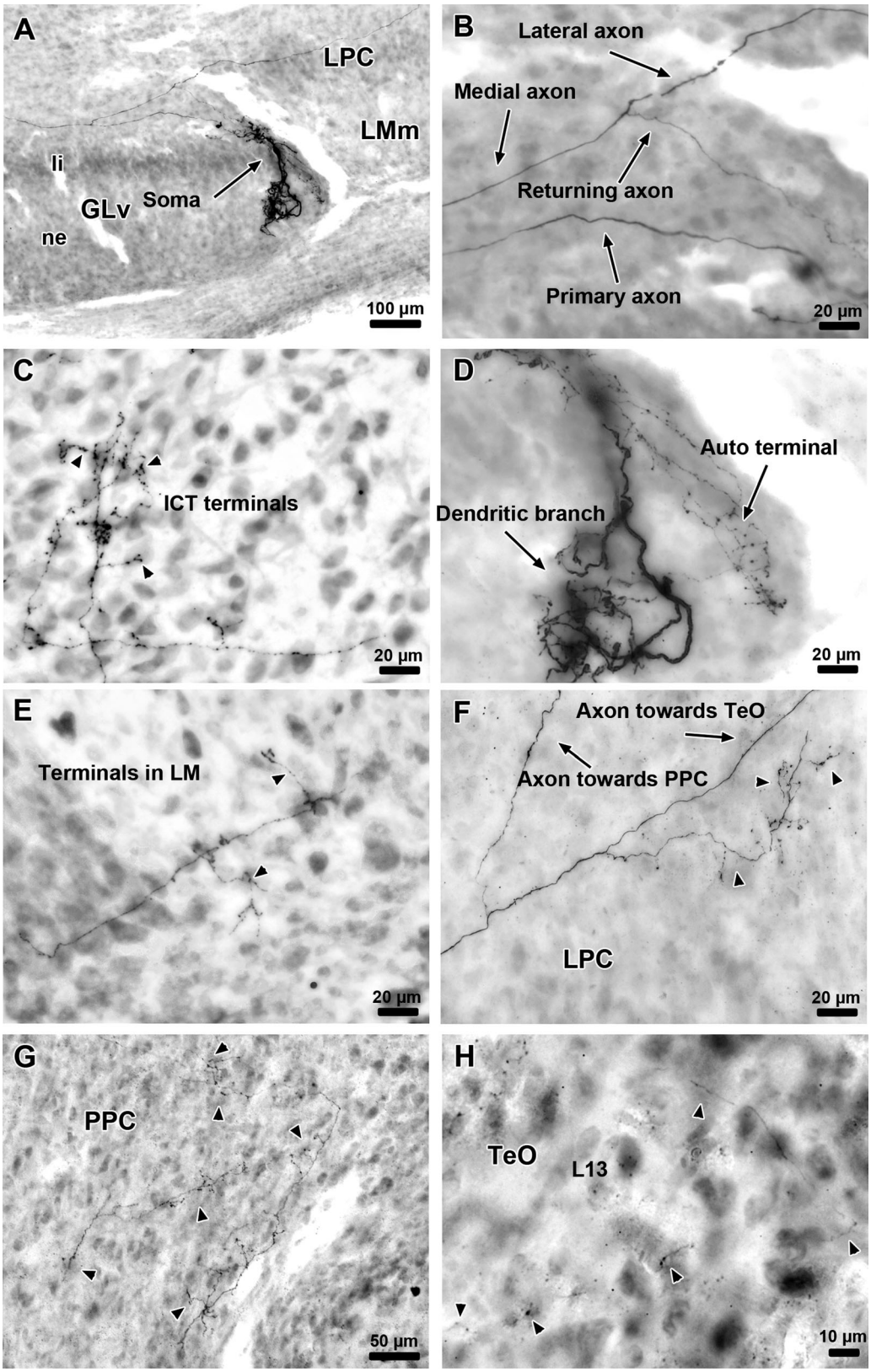

Figure 8. Intracellular filling of a representative GLv cell located in the lamina interna **(A). B–H**: The fine structure and different mesodiencephalic targets of two GLv-li cells. Arrowheads show terminals in the respective nuclei. Note the conspicuous autoterminal in the Glv-ne adjacent to the apical dendritic branch in (D). Also note the fine caliber terminal in layer 13 of the TeO in (H).

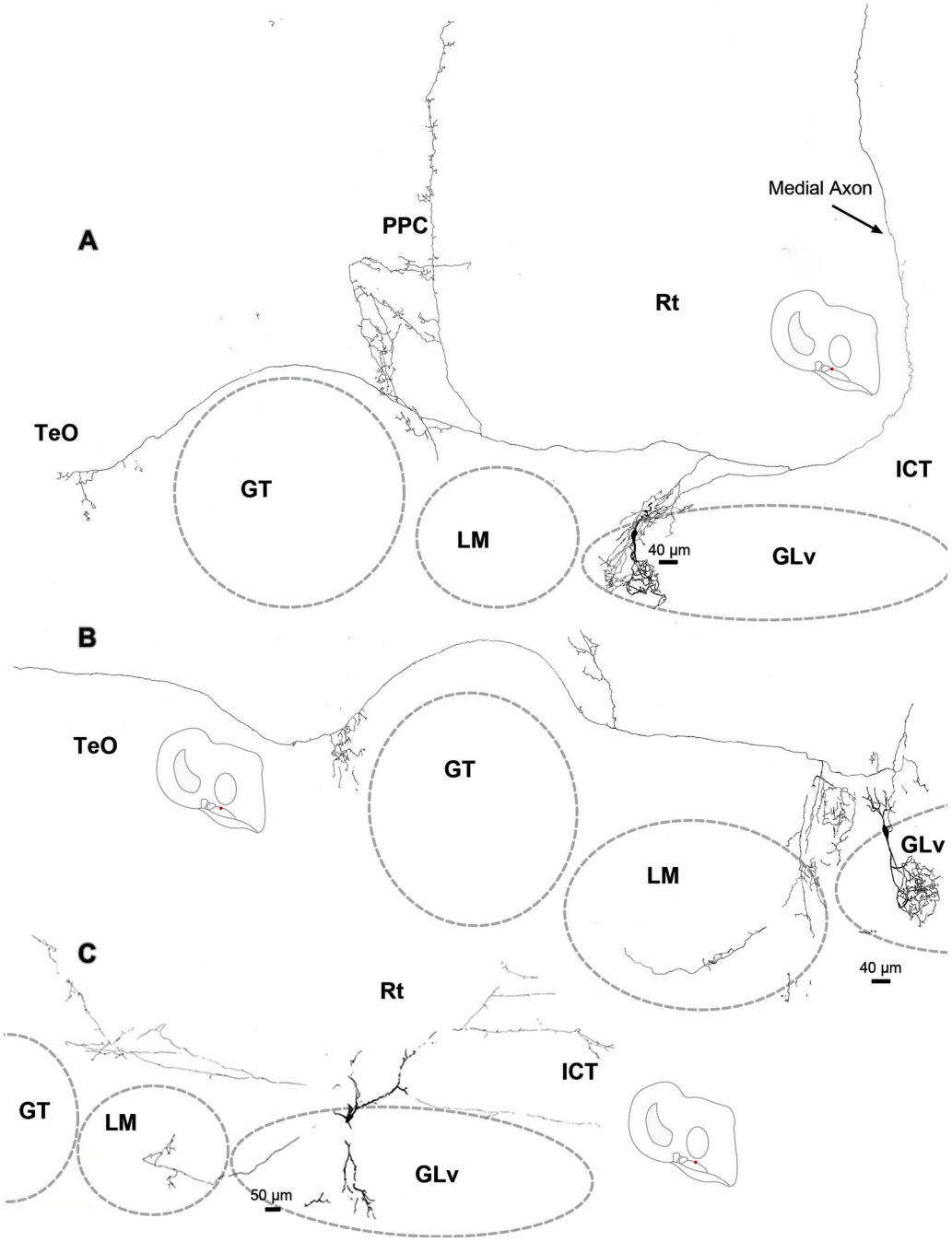

Figure 9. Reconstruction of biocytin-filled neurons in the lamina interna of the GLv. **A**: Cell showing an autoterminal in the neuropil of the GLv including a medial axon presumably projecting to PM in the hindbrain. **B**: Cell showing terminals in the LMm and the layer 13 of the TeO. **C**: Cell showing terminals in the LM and ICT. Insets with the dots indicate the location of each cell in a schematic slice. [Color figure can be viewed in the online issue, which is available at wileyonlinelibrary.com.]

All antisense probes used gave distinct labeling according to the assayed brain region, and the results were highly reproducible across different animals. Furthermore, no labeling was detected when the sense probes were used.

Our results showed that the pretectal GT, LM, and LPC had a strong expression of VGluT2 (Fig. 10A,C,E,F) but not VIAAT mRNA (Fig. 10B,D,G). This labeling was confined especially to the cells located in the GTc, LPC, and LMm/LMl; the GTv showed less intense expression, whereas the GLv showed a clear absence of VGluT2 expression (Fig. 10A,C,E,F). In contrast, a strong expression of VIAAT mRNA was found in the GLv (Fig. 10B,G). This labeling was observed in all cells of the GLv-li and in some dispersed cells of the neuropil. The

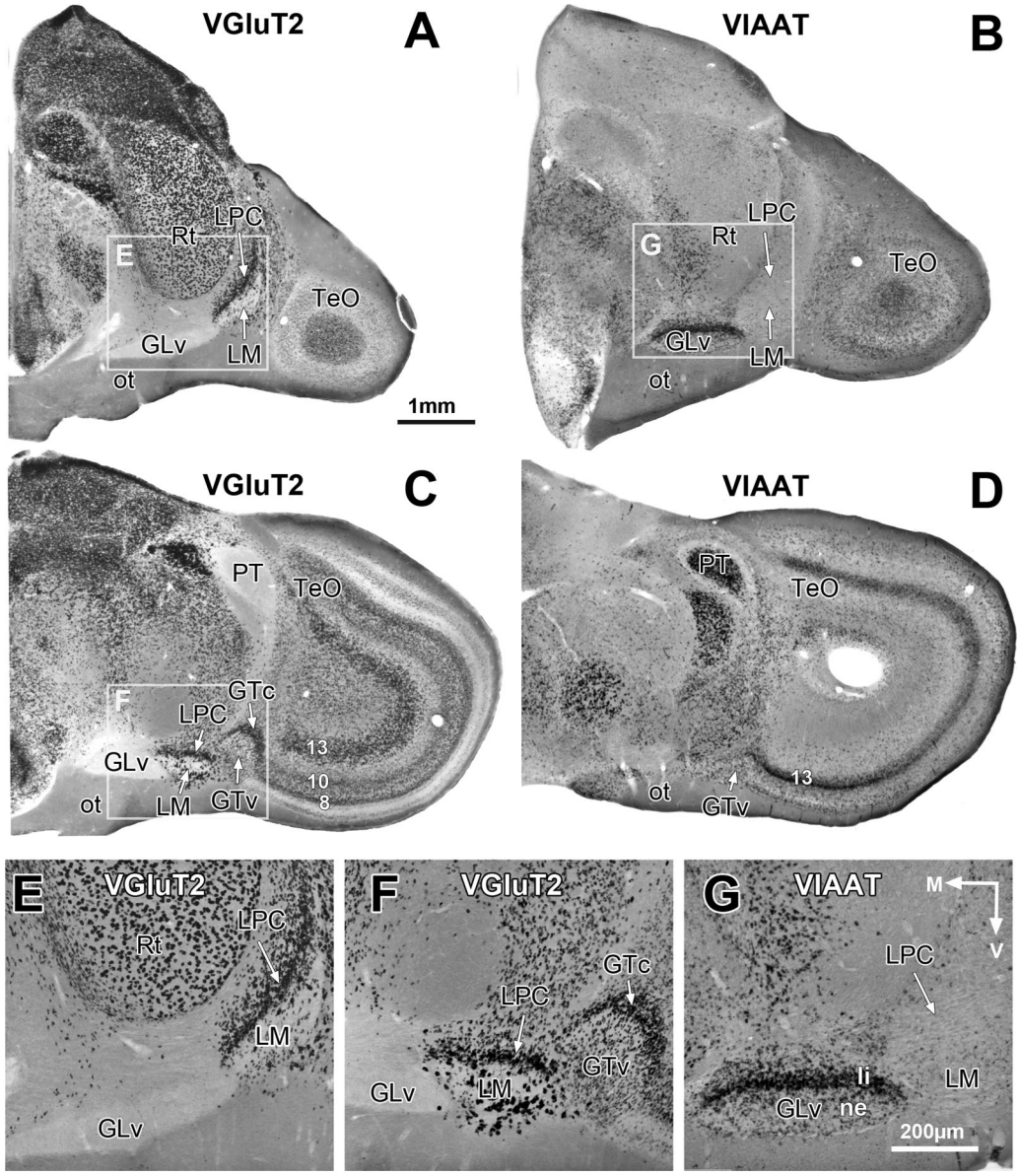

Figure 10. Coronal sections of the mesodiencephalic region with *in situ* hybridizations assays for vesicular glutamate transporter 2 (VGluT2) in **(A,C,E,F)** and inhibitory amino acid transporter (VIAAT) in **(B,D,G)**. The GT, LM, LPC, and tectal layers 8–10 and 13 strongly express the VGluT2 mRNA, as seen in (A,C). Note that the GLv is strongly labeled with the VIAAT mRNA probe and not with the VGLUT2 probe (E–G). This suggests an inhibitory phenotype for these neurons. The mRNA probes were revealed using the anti-digoxigenin antibody and the alkaline phosphatase reaction. Scale bar in A applies to B–D. Scale bar in G applies to E,F.

GT, LM, and LPC showed almost no expression (Fig. 10B,D,G). Nevertheless, as GABAergic and glycinergic functions share the VIAAT protein for their neurotransmitter vesicular intake, the sole expression is not sufficient for the identification of GABAergic phenotypes (Burger et al., 1991; Dumoulin et al., 1999). To disambiguate this, we performed *in situ* hybridization assays for glycine transporter 2 (GLYT2), which is the transporter responsible for increasing cytoplasmic glycine concentration in glycinergic cells. We found that GLYT2 was mainly expressed in the medullar and pontine structures and its expression was not detected in any of the structures studied including the GLv (data not shown). These results indicate that all VIAAT-positive neurons shown here are presumably GABAergic.

DISCUSSION

In this study we describe the morphology, microprojection pattern, and neurochemical identity of neurons located in the pretectal GT/LM/LPC and the ventrothalamic nucleus GLv in the chicken. Our data show that

these structures are strongly interconnected, specifically by neurons with large dendritic and axonal fields that span several nuclei. Neurons in the GLv express a GABAergic phenotype and have axonal projections that give rise to collateral fields in the ICT, LM, and in the deep layers of TeO. Neurons in the GT/LM/LPC are projection neurons with a glutamatergic phenotype. In the case of the GT, the axon proceeds to the TeO, LM, GLv, and ICT.

Slice preparation

Long and middle-range projections that contain somata and terminals of the same neurons are difficult to preserve in slice preparations because they often course beyond the physical limits of a regular slice (i.e., a slice cut along standard orientation planes). We found an unconventional plane of sectioning that resulted in slices that preserved the integrity of the ventral tecto-pretecto-ventrothalamic connection (Vega-Zuniga et al., 2014). Such a slice preparation, together with the relatively fast transport of biocytin (Horikawa and Armstrong, 1988; Izzo, 1991), allowed us to perform a detailed morphological and microprojection pattern analysis. Specifically, we were able to label cells with Golgi-like resolution. The results obtained in the slice were fully consistent and more informative, regarding the tecto-pretecto-ventrothalamic connection, than those previously obtained for *in vivo* experiments (Gamlin and Cohen, 1988b; Hu et al., 2004), further confirming the validity of the *in vitro* approach.

Morphology and projection pattern of the GT cells

Previous *in vivo* work using extracellular HRP injections in the GT (Gamlin and Cohen, 1988b) showed a projection to the tectum and the dorsal and ventral thalamus. We confirmed the GT projection to the GLv and add that it comes from at least two GT subpopulations (type I and II cells). The GT projection to the dorsal thalamus was not observed due to the fact that this connection is severed in the slice. Regarding the GT projection that proceeded to the TeO, our results are in agreement with the early work of Brecha (dissertation, 1978, cited by Gamlin and Cohen, 1988a) that showed a GT-TeO projection to the deep tectal layers (10–13). However, the more superficial projection to layer 4 mentioned in their work was not observed in our data. This may be due either to the cut of that terminal field in our slice preparation or to the uptake of HRP-tracer by nearby cells or passing fibers (Herkenham and Nauta, 1977), in the Gamlin and Cohen study, that projected to the superficial tectal layers. Our data add that the GT-TeO projection comes only from type I cells.

Interestingly, our results showed that GT-type I and II cells ended differentially in the LM/LPC and ventrothalamic area: the axons from GT-type I cells left collaterals that entered the LM/LPC from the dorsal part, then continued toward the ventrothalamic region and ended above the Glv-li and into the ICT. This latter structure also received GLv-li collaterals (Figs. 2C, 8C). The axons from type II cells, on the other hand, followed a ventral course above the optic tract and ended in the LM/LPC and GLv (Figs. 4B–H, 5C,D).

It is worth mentioning that GT projections to the TeO and GLv did not seem to be topographically organized but rather as axonal branches with different conduction delays. The presence of branch points and varicosities, as observed in our GT axons, reduces the conduction velocity (Debanne, 2004). In the case of the TeO, GT-collaterals ended in layer 13 probably onto SGC neurons (Fig. 3C,E), and in layer 10b possibly onto shepherd's crook (Sc) and/or vine neurons (Vega-Zuniga et al., 2014) (Fig. 3D). Regarding the role of these targeted cells, SGC neurons form part of the tectofugal pathway which has been linked to, e.g., luminance, color, motion, and looming (Wang et al., 1993); Sc neurons form part of the isthmo-tectal loop involved in visual attention (Marín et al., 2005; Asadollahi et al., 2011), and vine neurons project back to the GLv (Vega-Zuniga et al., 2014), which has been implicated in visuomotor control (Pateromichelakis, 1979; Guiloff et al., 1987). Furthermore, the GT is in receipt of direct retinal input (Gamlin and Cohen, 1988a). Hence, the GT projections over the TeO and GLv might be a source of specific temporal coding that may have crucial functional consequences for the visual operations in the TeO and GLv. Nevertheless, further physiological experiments are needed to confirm or discard this functional inference from our anatomical data.

Morphology of the LM and LPC cells

Neuroanatomical experiments have shown that the LM contains several cell types with different projection patterns, such as to the dorsal thalamus, nBOR, cerebellum, and inferior olive (Zayats et al., 2003; Pakan et al., 2006, 2010). In the present study we identified three different neuronal types located along the medial and lateral LM. These results were consistent with some of the different morphological types described by Pakan et al. (2006): e.g., our LM-type I cell seems to correspond to the small cells that either project to the nBOR, hippocampus, or dorsal thalamus, and LM-type II and III cells may correspond to the large multipolar neurons that project as mossy fibers to the vestibulocerebellum. Nevertheless, our LM-type III cell does not completely match the large multipolar neurons,

especially regarding the dense bipolar dendritic fields, which in Pakan's study (2006) were not observed. This could be due to the techniques used. *In vivo* tracing does not always fill the fine details of dendritic arbors as reliable as intracellular fillings, which have a Golgi-like labeling pattern.

Regarding the LM projection to the TeO, as previously reported by Gamlin and Cohen (1988b), none of our filled neurons showed a tectal collateral. This could be due to either axonal HRP-tracer uptake by GT cells (in the Gamlin and Cohen study) that innervate the LM and that project to the TeO, or that the axonal process was cut in our *in vitro* preparation. Likewise, the other known projections to the dorsal thalamus, nBOR, and the hindbrain were also not observed due to the absence of the dorsal and caudal connection in our slice.

Regarding the LPC, two neuronal types were filled in this adjacent structure to the LMm. These results are difficult to compare since previous studies did not showed detailed labeling of dendrites (Gamlin and Cohen, 1988b; Pakan et al., 2006). Nevertheless, some interesting issues arose in our data with respect to the LMm and the adjacent structure LPC. Previous work has considered the LMm and LPC as different nuclei (Gamlin and Cohen, 1988a,b). This assumption was also supported by the projection pattern: LPC cells project to the medial pons (Gamlin and Cohen, 1988b), whereas the LMm cells project to the cerebellum and inferior olive (Pakan et al., 2006, 2010). However, Gamlin and Cohen (1988b) suggested that the relationship between them is equivalent to that between the lamina interna and neuropil of the GLv, i.e., the soma lies in the GLv-li and the dendrites extend into the GLv-ne where retinal terminals end. Our filled cells located in the LPC confirm this, since they showed a dense and extensive dendritic arbor into the retinorecipient LMm (Fig. 6B). In addition, cells located in the GLv-ne also have axons that leave the nucleus (unpublished observation) as in the case of the LMm cells that project to the cerebellum and inferior olive. Nevertheless, note that in our preparation only the ventral part of the LM was present. Thus, these data should be assessed with care since they are not necessarily representative of all cells of the LM complex. Therefore, further experiments of the complete LMm and LPC nuclei will be needed in order to confirm or disprove our observations.

Morphology and projection pattern of GLv-li cells

Previous work identified five different cell types in the GLv, including a specific cell type that predominates in the GLv-li (Guiloff et al., 1987; Tömböl et al., 2004). Although in general our results are in agreement with these previous observations, our morphological data differ slightly regarding the dendritic extension and axonal projection of the GLv-li cells. We interpret these results as a consequence of the slice limitations and not as the presence of another cell type. The soma-dendritic profile of the GLv-li neurons extended over 500–600 microns, which was the slice thickness used. As a result, part of the cellular morphology was lost when a filled neuron was located more superficially. Hence, the morphological dendritic and axonal variation observed in our study depended on the depth of the filled neuron in the slice.

Regarding the projection pattern, GLv-li cells showed a very complex connectivity that included different dendritic arbors and axon collaterals. Each individual neuron projects to the LM, GT, TeO, PPC, and ICT, along with an axon that presumably ends in the PM (Marín et al., 2001). Additionally, these neurons exhibited a remarkable peculiarity: the presence of an axon collateral that fed back and arborized within the GLv-ne. This auto-terminal did not overlap completely with the dendritic field of the same neuron, but with its neighboring dendritic area (Fig. 8D). GABAergic neurons with similar local axonal network have been previously described in the sensory-motor subdivision of the rat substantia nigra pars reticulata (SNR) (Mailly et al., 2003). These cells form the main output of nuclei of the basal ganglia that conveys the striatal outflow to brainstem premotor networks and thalamic nuclei. Consequently, the morphological and neurochemical similarities including the connectivity with premotor areas between the SNR and GLv-li neurons reinforce the idea of a putative sensorimotor role for the GLv.

Finally, it is of interest to mention that the GLv-TeO projection has been discussed since the 1980s. Several reports suggested the existence of a reciprocal topographic connection between both structures (Maturana and Varela, 1982; Guiloff et al., 1987), although it has been pointed out that the GLv-TeO projection is not topographic and does not form a substantial organized connection as the TeO-GLv (Vega-Zuniga et al., 2014). This inconsistency might be due to differential injection depths used. In our study, retrogradely labeled GLv-li neurons only occurred after localized extracellular injections in the deep layer 13 of the TeO (data not shown). In contrast, previous *in vivo* tectal injections (Crossland and Uchwat, 1979; Wylie et al., 2009) were preferentially made in the intermediate layers. Hence, it is probably due to the deep location and the fine caliber of the GLv terminals in the TeO that these *in vivo* tectal injections did not yield to consistent and topographic retrograde labeling in the GLv. Our results suggest that

the GLv-TeO connection may indeed form an organized and functional projection that ends in the deep tectal layers.

Neurochemical identity of the pretecto-ventrothalamic circuit

Immunohistochemical localization of diverse markers and mRNA expression of different probes have been studied in the avian brain (Güntürkün and Karten, 1991; Heyers et al., 2004, 2008; Mukherjee and Hausman, 2004; Sun et al., 2005). In general, the expression patterns detected by our mRNA probes are in agreement with previous reports on glutamatergic (Islam and Atoji, 2008; González-Cabrera et al., 2015) and GABAergic (Domenici et al., 1988; Veenman and Reiner, 1994; Sun et al., 2005) neuronal distribution in the avian brain. Specifically, the pretectal nuclei GT, LM and LPC showed a marked glutamatergic expression in the GTc, LMl, and LMm. Although we did not perform double-labeling experiments, the conspicuous expression observed strongly suggests that our filled neurons in these pretectal structures are predominantly glutamatergic.

On the other hand, the high VIAAT mRNA expression in the GLv-li and some neurons in the GLv-ne indicate a vesicular transporter for an inhibitory amino acid. Moreover, the absence of the GLYT2 mRNA expression suggests a GABAergic transmission. Hence, the GLv-li projection neurons described in this study suggest that they are GABA-positive and therefore presumably inhibitory. These results together with previous work (Güntürkün and Karten, 1991; Veenman and Reiner, 1994; Sun et al., 2005) confirm the GABAergic identity for the GLv. Yet other neurotransmitter involvement cannot be ruled out.

Synaptic interactions of the pretecto-ventrothalamic network

The GLv, LM, and GT receive topographic retinal projections from different retinal ganglion cell populations (Crossland and Uchwat, 1979; Gamlin and Cohen, 1988a; Wylie et al., 2014), which may release glutamate in all these structures (Guo et al., 1998; Atoji, 2011). At the same time, AMPA receptors GluR1, GluR2/3, and GluR4 are expressed in the GT, LM, and GLv (Pires and Britto, 1997). Thus, the retinal input may form direct synaptic contact with the somata and dendrites of the various cell types located within these structures.

In addition, our results together with previous work (Islam and Atoji, 2008) strongly suggests a glutamatergic identity of the cells located in the GT, LM, and LPC. Thus, the different projection cell types of the LM/LPC are likely to have glutamatergic synapses with the dorsal thalamus, nBOR, inferior olive, cerebellum, and pons, respectively. Whereas cells located in the GT probably have glutamatergic synapses with the GLv, LM/LPC, and TeO. Furthermore, layers 10 and 13 of the TeO, which are layers where GT projections end, showed moderate to intense expression of the receptor GluR2/3 (Pires and Britto, 1997). The dual projection pattern of the GT to the LM/LPC and GLv, that is, GT-type I cell axons distributing terminals from dorsal and GT-type II cells axons from ventral, may imply different cellular targets. Very likely, the ventral projection ends in the retinal terminals of LMm/GLv-ne, while the dorsal projection contacts the projection cells of the GLv-li and LM/LPC. Finally, the GLv here characterized as predominantly GABAergic contains GLv-li neurons with large dendritic and axonal fields that span several nuclei. Consistently, $GABA_B$ receptors are expressed in the GT, LM, and layers 7–13 of the TeO (Veenman et al., 1994) where GLv terminals end.

Therefore, as a group (and taking the current literature into account), the pretecto-ventrothalamic nuclei are retinorecipient structures highly interconnected between each other and with the tecto- and thalamofugal pathways. In general terms, this network is mainly composed of pretectal glutamatergic and ventrothalamic GABAergic neurons (Fig. 11). The receptors found in these nuclei also suggest that there are indeed excitatory and inhibitory synapses between them. If so, the GLv would exert inhibition and the GT and LM/LPC would exert excitation upon the respectively targeted structures.

Functional role of the pretecto-ventrothalamic network

The role of the LM in optic flow is generally accepted, yet the function of the GT remains unknown and the role of the GLv is still controversial. However, regarding the ventral thalamus, a previous optomotor study revealed some clues about the GLv function. Gioanni et al. (1991) showed that unilateral lesion with kainic acid (which does not damage fibers of passage; Coyle et al., 1978; Sperk, 1994) in the GLv produced an enhancement of the horizontal optokinetic response in pigeons, suggesting an inhibitory input. Since this reflex is known to be mediated by the LM (Simpson, 1984; McKenna and Wallman, 1985), a tight link between the GLv-LM was suggested. Remarkably, our data support the aforementioned study in two important aspects: first, there is indeed a topographic projection from the GLv to LM, and second, the connection is very likely GABAergic. Consequently, all these findings strengthen the idea of a visuomotor role of the GLv (Pateromichelakis, 1979; Guiloff et al., 1987).

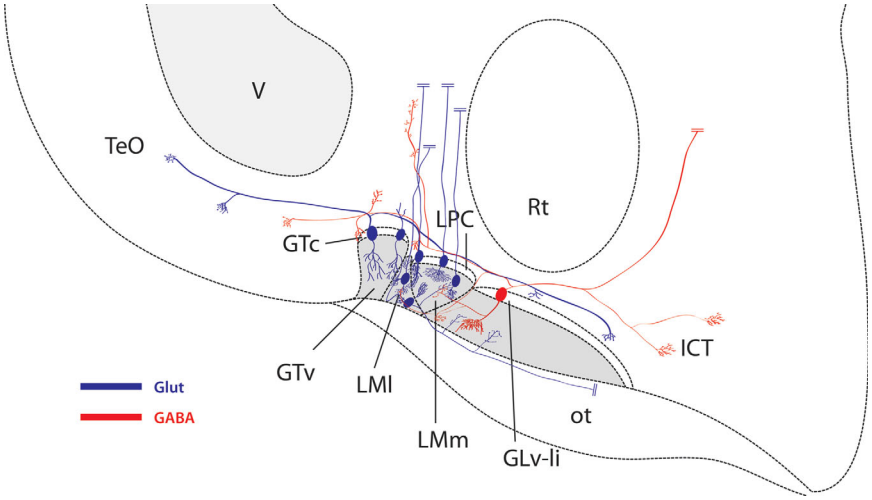

Figure 11. Schematic drawing of the proposed neural circuitry of the pretecto-GLv connection. Glutamatergic neurons are located in the GT, LM, and LPC (blue). GABAergic neurons are found in the GLv (red). Parallel lines (red and blue) at the end of the axons indicate the continuity of the axon beyond the limits of the slice. The gray shading indicates the retinorecipient region in the GT, LM, and GLv. Note that GTc, LPC, and GLv-li are free of retinal terminals.

On a more global view, it seems that the ventral thalamus and pretectum are part of a broader sensorimotor network. The literature and the detailed mesodiencephalic microconnectomics presented in our study strongly suggest that the GLv, LM/LPC, and GT are part of a concerted visuomotor circuit that further includes the TeO, pons, and cerebellum. Specifically, the GLv has a cholinergic tectal afferent which may modulate the retinal terminals in this nucleus (Medina and Reiner, 1994; Vega-Zuniga et al., 2014). Additionally, the GLv, LM, ICT, and TeO project to the pons (Gamlin and Cohen, 1988b; du Lac and Knudsen, 1990; Marín et al., 2001; Wylie et al., 2009). The pontine nuclei, in turn, proceed to the cerebellar vermis at the level of the visuomotor folia VIc-IXc (Freedman et al., 1975; Clarke, 1977). Finally, the cerebellum, via the lateral cerebellar nucleus, projects back to the GLv, ICT, and PM, among other structures (Arends and Zeigler, 1991).

Hence, the evidence suggests that these apparently dissimilar nuclei distributed along the mesencephalon, diencephalon, and rhombencephalon are part of a larger and sophisticated interconnected network that enables specific visuomotor functions such as generation/modulation of saccades, pursuits, corollary discharge, and gaze control. Further detailed physiological and behavioral studies will be needed to confirm the validity of these assumptions.

Comparison to mammals

In birds and mammals, the ventrothalamic and pretectal nuclei receive a significant retinal input (Gamlin and Cohen, 1988a; Major et al., 2003; Vega-Zuniga et al., 2013; Krabichler et al., 2015). Also, these structures show a projection pattern that is very similar in both groups. A characteristic feature regarding the ventrothalamic complex is that it has no further projections to the telencephalon, while it sends descending efferents towards the pretectum, tegmentum, and pontine nuclei (Harrington, 1997; Marín et al., 2001). In mammals, the GLv complex receives afferents from the retina, optic tectum (superior colliculus), cortex, and cerebellum (Harrington, 1997). Efferents from this complex project to the optic tectum, zona incerta, pretectum, accessory optic nuclei, medial pons, and motor tegmentum (Harrington, 1997). In birds, the literature regarding this complex (LA, IGL, VLT/ICT, and GLv) is scant. However, the overall pattern of connections is similar to that of mammals, i.e., the GLv projection to the PM, TeO, and the cerebellar projection back to the GLv (Arends and Zeigler, 1991). It is worth noting that our study shows for the first time a clear GLv-TeO projection in birds. This finding is relevant in comparative terms because it argues in favor of a conserved reciprocal functional GLv-TeO connectivity between mammals and birds. In addition, the retino-recipient pretectal nuclei also form a complex of nuclei that are presumably conserved in phylogeny. Based on physiology, histochemistry, and lesion studies, various authors have suggested that the LM of birds is homologous to the nucleus of the optic tract in mammals (Simpson, 1984; McKenna and Wallman, 1985). On the other hand, the GT is comparable to the posterior pretectal nucleus in rats. This latter suggestion was based on hodological

studies showing that they share projections to the GLv and the optic tectum (Gamlin and Cohen, 1988b). However, a more thorough comparison cannot be made because of the scarcity of physiological and behavioral studies in both birds and mammals. Thus, by clarifying the cellular morphology, neurochemistry, and connectivity of these nuclei in the chick, our study paves the way for future comparative studies aiming to resolve the physiology and role of the meso-diencephalic network in both birds and mammals.

SUMMARY

We used intracellular filling and *in situ* hybridization assays to characterize the morphology, projection pattern, and neurochemical identity of neurons of the GT, LM/LPC, and GLv. Our data indicate a complex connectivity pattern between these structures, including GLv and GT neuronal axons that span several nuclei. Furthermore, the pretectal nuclei have a glutamatergic identity and the GLv has a GABAergic identity. We propose that this complex morphology and connectivity pattern might be the structural organization necessary to coordinate specific orienting visuomotor behaviors and the optic flow patterns that they induce.

ACKNOWLEDGMENTS

We thank Birgit Seibel, Yvonne Schwarz, Gaby Schwabedissen for excellent technical assistance, and Dr. Cristian Gutierrez-Ibanez and Quirin Krabichler for critically reading the article.

CONFLICT OF INTEREST

The authors declare no conflicts of interest.

AUTHOR CONTRIBUTIONS

All authors had full access to all data in the study and take responsibility for the integrity of the data and the accuracy of the data analysis. Study concept and design: TVZ, GM, CGC, JM, HL. Acquisition of data: TVZ, AH, EP, VM, CGC. Analysis and interpretation of data: TVZ, GM, CGC, AH, EP, VM, JM, HL. Drafting of the article: TVZ, GM, CGC, JM, HL. Critical revision of the article for important intellectual content: GM, JM, HL. Administrative, technical, and material support: HL, GM.

LITERATURE CITED

Arends JJ, Zeigler HP. 1991. Organization of the cerebellum in the pigeon (Columba livia): II. Projections of the cerebellar nuclei. J Comp Neurol 306:245–272.

Asadollahi A, Mysore SP, Knudsen EI. 2011. Rules of competitive stimulus selection in a cholinergic isthmic nucleus of the owl midbrain. J Neurosci 31:6088–6097.

Atoji Y. 2011. Immunohistochemical localization of vesicular glutamate transporter 2 (vGluT2) in the central nervous system of the pigeon (Columba livia). J Comp Neurol 519:2887–2905.

Bell-Pedersen D, Cassone VM, Earnest DJ, Golden SS, Hardin PE, Thomas TL, Zoran MJ. 2005. Circadian rhythms from multiple oscillators: lessons from diverse organisms. Nat Rev Genet 6:544–556.

Bishop PO, Pettigrew JD. 1986. Neural mechanisms of binocular vision. Vision Res 26:1587–1600.

Brandstätter DR, Abraham U. 2003. Hypothalamic circadian organization in birds. I. Anatomy, functional morphology, and terminology of the suprachiasmatic region. Chronobiol Int 20:637–655.

Buijs RM, Kalsbeek A. 2001. Hypothalamic integration of central and peripheral clocks. Nat Rev Neurosci 2:521–526.

Burger PM, Hell J, Mehl E, Krasel C, Lottspeich F, Jahn R. 1991. GABA and glycine in synaptic vesicles: storage and transport characteristics. Neuron 7:287–293.

Butler AB, Hodos W. 2005. Comparative vertebrate neuroanatomy: evolution and adaptation. Hoboken, NJ: John Wiley & Sons.

Cantwell EL, Cassone VM. 2006. Chicken suprachiasmatic nuclei. I. Efferent and afferent connections. J Comp Neurol 496:97–120.

Clarke PG. 1977. Some visual and other connections to the cerebellum of the pigeon. J Comp Neurol 174:535–552.

Coyle JT, Molliver ME, Kuhar MJ. 1978. In situ injection of kainic acid: a new method for selectively lesioning neural cell bodies while sparing axons of passage. J Comp Neurol 180:301–323.

Crapse TB, Sommer MA. 2008. Corollary discharge across the animal kingdom. Nat Rev Neurosci 9:587–600.

Crossland WJ, Uchwat CJ. 1979. Topographic projections of the retina and optic tectum upon the ventral lateral geniculate nucleus in the chick. J Comp Neurol 185:87–106.

Crowder NA, Lehmann H, Parent MB, Wylie DRW. 2003. The accessory optic system contributes to the spatio-temporal tuning of motion-sensitive pretectal neurons. J Neurophysiol 90:1140–1151.

Debanne D. 2004. Information processing in the axon. Nat Rev Neurosci 5:304–316.

Domenici L, Waldvogel HJ, Matute C, Streit P. 1988. Distribution of GABA-like immunoreactivity in the pigeon brain. Neuroscience 25:931–950.

du Lac S, Knudsen EI. 1990. Neural maps of head movement vector and speed in the optic tectum of the barn owl. J Neurophysiol 63:131–146.

Dumoulin A, Rostaing P, Bedet C, Levi S, Isambert M, Henry J, Triller A, Gasnier B. 1999. Presence of the vesicular inhibitory amino acid transporter in GABAergic and glycinergic synaptic terminal boutons. J Cell Sci 112:811–823.

Freedman SL, Feirabend HK, Vielvoye GJ, Voogd J. 1975. Re-examination of the ponto-cerebellar projection in the adult white leghorn (Gallus domesticus). Acta Morphol Neerl Scand 13:236–238.

Frost BJ, Cavanagh P, Morgan B. 1988. Deep tectal cells in pigeons respond to kinematograms. J Comp Physiol A 162:639–647.

Gamlin PD, Cohen DH. 1988a. Retinal projections to the pretecturn in the pigeon (Columba livia). J Comp Neurol 17: 1–17.

Gamlin PD, Cohen DH. 1988b. Projections of the retinorecipient pretectal nuclei in the pigeon (Columba livia). J Comp Neurol 269:18–46.

Gioanni H, Palacios A, Sansonetti A, Varela F. 1991. Role of the nucleus geniculatus lateralis ventralis (GLv) in the optokinetic reflex: a lesion study in the pigeon. Exp Brain Res 86:601–607.

González-Cabrera C, Garrido-Charad F, Roth A, Marín GJ. 2015. The isthmic nuclei providing parallel feedback connections to the avian tectum have different neurochemical identities: expression of glutamatergic and cholinergic markers in the chick (Gallus gallus). J Comp Neurol 523:1341–1358.

Guiloff GD, Maturana HR, Varela FJ. 1987. Cytoarchitecture of the avian ventral lateral geniculate nucleus. J Comp Neurol 264:509–526.

Güntürkün O, Karten HJ. 1991. An immunocytochemical analysis of the lateral geniculate complex in the pigeon (Columba livia). J Comp Neurol 314:721–749.

Guo JZ, Tredway TL, Chiappinelli VA. 1998. Glutamate and GABA release are enhanced by different subtypes of presynaptic nicotinic receptors in the lateral geniculate nucleus. J Neurosci 18:1963–1969.

Guo J-Z, Liu Y, Sorenson EM, Chiappinelli VA. 2005. Synaptically released and exogenous ACh activates different nicotinic receptors to enhance evoked glutamatergic transmission in the lateral geniculate nucleus. J Neurophysiol 94:2549–2560.

Guo JZ, Sorenson EM, Chiappinelli VA. 2010. Cholinergic modulation of non-N-methyl-D-aspartic acid glutamatergic transmission in the chick ventral lateral geniculate nucleus. Neuroscience 166:604–614.

Harrington ME. 1997. The ventral lateral geniculate nucleus and the intergeniculate leaflet: interrelated structures in the visual and circadian systems. Neurosci Biobehav Rev 21:705–727.

Herkenham M, Nauta WJ. 1977. Afferent connections of the habenular nuclei in the rat. A horseradish peroxidase study, with a note on the fiber-of-passage problem. J Comp Neurol 173:123–146.

Heyers D, Luksch H, Redies C. 2004. Selective synaptic cadherin expression by traced neurons of the chicken visual system. Neuroscience 127:901–912.

Heyers D, Manns M, Luksch H, Güntürkün O, Mouritsen H. 2008. Calcium-binding proteins label functional streams of the visual system in a songbird. Brain Res Bull 75: 348–355.

Horikawa K, Armstrong WE. 1988. A versatile means of intracellular labeling: injection of biocytin and its detection with avidin conjugates. J Neurosci Methods 25:1–11.

Hu M, Naito J, Chen Y, Ohmori Y, Fukuta K. 2004. Afferent and efferent connections of the nucleus geniculatus lateralis ventralis demonstrated by WGA-HRP in the chick. Anat Histol Embryol 33:192–195.

Islam MR, Atoji Y. 2008. Distribution of vesicular glutamate transporter 2 and glutamate receptor 1 mRNA in the central nervous system of the pigeon (Columba livia). J Comp Neurol 511:658–677.

Iwaniuk AN, Pakan JMP, Gutiérrez-Ibáñez C, Wylie DR. 2009. Expression of calcium-binding proteins in cerebellar- and inferior olivary-projecting neurons in the nucleus lentiformis mesencephali of pigeons. Vis Neurosci 26:341–347.

Izzo PN. 1991. A note on the use of biocytin in anterograde tracing studies in the central nervous system: application at both light and electron microscopic level. J Neurosci Methods 36:155–166.

Kaas JH, Lyon DC. 2007. Pulvinar contributions to the dorsal and ventral streams of visual processing in primates. Brain Res Rev 55:285–296.

Karten HJ, Revzin AM. 1966. The afferent connections of the nucleus rotundus in the pigeon. Brain Res 2:368–377.

Karten HJ, Hodos W, Nauta WJ, Revzin AM. 1973. Neural connections of the "visual wulst" of the avian telencephalon. Experimental studies in the piegon (Columba livia) and owl (Speotyto cunicularia). J Comp Neurol 150:253–278.

Krabichler Q, Vega-Zuniga T, Morales C, Luksch H, Marín GJ. 2015. The visual system of a Palaeognathous bird: visual field, retinal topography and retino-central connections in the Chilean Tinamou (Nothoprocta perdicaria). J Comp Neurol 523:226–250.

Luksch H. 2003. Cytoarchitecture of the avian optic tectum: neuronal substrate for cellular computation. Rev Neurosci 14:85–106.

Mailly P, Charpier S, Menetrey A, Deniau J-M. 2003. Three-dimensional organization of the recurrent axon collateral network of the substantia nigra pars reticulata neurons in the rat. J Neurosci 23:5247–5257.

Major DE, Rodman HR, Libedinsky C, Karten HJ. 2003. Pattern of retinal projections in the California ground squirrel (Spermophilus beecheyi): anterograde tracing study using cholera toxin. J Comp Neurol 463:317–340.

Marín G, Henny P, Letelier JC, Sentis E, Karten H, Mrosko B, Mpodozis J. 2001. A simple method to microinject solid neural tracers into deep structures of the brain. J Neurosci Methods 106:121–129.

Marín G, Letelier JC, Henny P, Sentis E, Farfán G, Fredes F, Pohl N, Karten H, Mpodozis J. 2003. Spatial organization of the pigeon tectorotundal pathway: an interdigitating topographic arrangement. J Comp Neurol 458:361–380.

Marín G, Mpodozis J, Mpdozis J, Sentis E, Ossandón T, Letelier JC. 2005. Oscillatory bursts in the optic tectum of birds represent re-entrant signals from the nucleus isthmi pars parvocellularis. J Neurosci 25:7081–7089.

Masino T, Knudsen EI. 1993. Orienting head movements resulting from electrical microstimulation of the brainstem tegmentum in the barn owl. J Neurosci 13:351–370.

Maturana HR, Varela FJ. 1982. Color-opponent responses in the avian lateral geniculate: a study in the quail (Coturnix coturnix japonica). Brain Res 247:227–241.

McKenna OC, Wallman J. 1985. Accessory optic system and pretectum of birds: comparisons with those of other vertebrates (Part 2 of 2). Brain Behav Evol 26:104–116.

Medina L, Reiner A. 1994. Distribution of choline acetyltransferase immunoreactivity in the pigeon brain. J Comp Neurol 342:497–537.

Mukherjee RS, Hausman RE. 2004. Cloning of chicken choline acetyltransferase and its expression in early embryonic retina. Brain Res Mol Brain Res 129:54–66.

Pakan JMP, Krueger K, Kelcher E, Cooper S, Todd KG, Wylie DRW. 2006. Projections of the nucleus lentiformis mesencephali in pigeons (Columba livia): a comparison of the morphology and distribution of neurons with different efferent projections. J Comp Neurol 495:84–99.

Pakan JMP, Graham DJ, Wylie DR. 2010. Organization of visual mossy fiber projections and zebrin expression in the pigeon vestibulocerebellum. J Comp Neurol 518:175–198.

Pateromichelakis S. 1979. Response properties of units in the lateral geniculate nucleus of the domestic chick (Gallus domesticus). Brain Res 167:281–296.

Pettigrew JD. 1986. The evolution of binocular vision. In: Pettigrew JD, Sanderson KJ, Levick WR, editors. Visual neuroscience. Cambridge, UK: Cambridge University Press. p 208–222.

Pires RS, Britto LRG. 1997. Distribution of AMPA-type glutamate receptor subunits in the chick visual system. Brazilian J Med Biol Res 30:73–77.

Reese BE, Cowey A. 1983. Projection lines and the ipsilateral retino-geniculate pathway in the hooded rat. Neuroscience 10:1233–1247.

Rodieck RW. 1979. Visual pathways. Annu Rev Neurosci 2: 193–225.

Rusak B, Zucker I. 1979. Neural regulation of circadian rhythms. Physiol Rev 59.

Simpson JI. 1984. The accessory optic system. Annu Rev Neurosci 7:13–41.

Sperk G. 1994. Kainic acid seizures in the rat. Prog Neurobiol 42:1–32.

Stephan FK, Zucker I. 1972. Circadian rhythms in drinking behavior and locomotor activity of rats are eliminated by hypothalamic lesions. Proc Natl Acad Sci U S A 69: 1583–1586.

Sun Z, Wang HB, Laverghetta A, Yamamoto K, Reiner A. 2005. The distribution and cellular localization of glutamic acid decarboxylase-65 (GAD65) mRNA in the forebrain and midbrain of domestic chick. J Chem Neuroanat 29:265–281.

Tömböl T, Eyre M, Zayats N, Németh A. 2004. The internal structure of the nucleus geniculatus lateralis ventralis in the avian brain: a Golgi study and electron microscopic investigation. Cells Tissues Organs 177:237–256.

Veenman CL, Reiner A. 1994. The distribution of GABA-containing perikarya, fibers, and terminals in the forebrain and midbrain of pigeons, with particular reference to the basal ganglia and its projection targets. J Comp Neurol 339:209–250.

Veenman CL, Albin RL, Richfield EK, Reiner A. 1994. Distributions of GABA(A), GABA(B), and benzodiazepine receptors in the forebrain and midbrain of pigeons. J Comp Neurol 344:161–189.

Vega-Zuniga T, Medina FS, Fredes F, Zuniga C, Severín D, Palacios AG, Karten HJ, Mpodozis J. 2013. Does nocturnality drive binocular vision? Octodontine rodents as a case study. PLoS One 8:e84199.

Vega-Zuniga T, Mpodozis J, Karten HJ, Marín G, Hain S, Luksch H. 2014. Morphology, projection pattern, and neurochemical identity of Cajal's "centrifugal neurons": the cells of origin of the tectoventrogeniculate pathway in pigeon (Columba livia) and chicken (Gallus gallus). J Comp Neurol 522:2377–2396.

Wang Y-C, Jiang S, Frost BJ. 1993. Visual processing in pigeon nucleus rotundus: Luminance, color, motion, and looming subdivisions. Vis Neurosci 10:21–30.

Wylie D. 2000. Binocular neurons in the nucleus lentiformis mesencephali in pigeons: responses to translational and rotational optic flowfields. Neurosci Lett 291:9–12.

Wylie DRW. 2001. Projections from the nucleus of the basal optic root and nucleus lentiformis mesencephali to the inferior olive in pigeons (Columba livia). J Comp Neurol 429:502–513.

Wylie DRW, Crowder NA. 2000. Spatiotemporal properties of fast and slow neurons in the pretectal nucleus lentiformis mesencephali in pigeons. J Neurophysiol 84:2529–2540.

Wylie D, Frost B. 1999. Responses of neurons in the nucleus of the basal optic root to translational and rotational flowfields. J Neurophysiol 81:267–276.

Wylie DR, Linkenhoker B, Lau KL. 1997. Projections of the nucleus of the basal optic root in pigeons (Columba livia) revealed with biotinylated dextran amine. J Comp Neurol 384:517–536.

Wylie DRW, Gutierrez-Ibanez C, Pakan JMP, Iwaniuk AN. 2009. The optic tectum of birds: mapping our way to understanding visual processing. Can J Exp Psychol 63:328–338.

Wylie DR, Kolominsky J, Graham DJ, Lisney TJ, Gutierrez-Ibanez C. 2014. Retinal projection to the pretectal nucleus lentiformis mesencephali in pigeons (Columba livia). J Comp Neurol 522:3928–3942.

Xu X, Ichida JM, Allison JD, Boyd JD, Bonds AB, Casagrande VA. 2001. A comparison of koniocellular, magnocellular and parvocellular receptive field properties in the lateral geniculate nucleus of the owl monkey (Aotus trivirgatus). J Physiol 531:203–218.

Yang Y, Cao P, Yang Y, Wang S-R. 2008. Corollary discharge circuits for saccadic modulation of the pigeon visual system. Nat Neurosci 11:595–602.

Zayats N, Eyre MD, Némeh A, Tömböl T. 2003. The intrinsic organization of the nucleus lentiformis mesencephali magnocellularis: a light- and electron-microscopic examination. Cells Tissues Organs 174:194–207.